UILU-ENG 91-3604

Report No. 158

NONPROPORTIONAL BIAXIAL FATIGUE OF WELDED JOINTS

by

Olli Aslak Siljander, P. Kurath and F. V. Lawrence

A Report of the

MATERIALS ENGINEERING—MECHANICAL BEHAVIOR

College of Engineering, University of Illinois at Urbana-Champaign

December 1991

NONPROPORTIONAL BIAXIAL FATIGUE OF WELDED JOINTS

Olli Aslak Siljander, Ph.D.
Department of Mechanical and Industrial Engineering
University of Illinois at Urbana-Champaign, 1991

ABSTRACT

The proportional and nonproportional high-cycle fatigue behavior of mild-steel, tube-to-plate welded specimens was studied. In-phase bending and torsion, constant-amplitude fatigue tests were used to define the weldment baseline material properties and also to serve as a comparison with out-of-phase tests. In-phase, combined bending-torsion experiments were conducted on the tube-to-plate specimen to simulate the common laboratory tests involving stationary loads on a beam. Out-of-phase combined bending-torsion loading paths were generated for a tube-to-plate specimen to simulate cyclic stress states typical of highway bridge beams subjected to a single passage of a vehicle.

The fatigue life of the tube-to-plate weldments was found to be load-path dependent for a bending-to-shear-stress ratio $\lambda = 2.39$. For the load history considered, in-phase loading was found to give an order of magnitude longer fatigue life than an out-of-phase loading having the same principal stress amplitudes. Approximately 80% of the total fatigue life of the tube-to-plate weldments was spent in initiating fatigue cracks in the life regime of 10^5 to 10^7 cycles for all loading paths studied.

The fatigue test results were correlated with various multiaxial fatigue damage parameters based on the local, notch-root stresses from finite element analyses of the weld-toe notches. The tests results for both the in-phase and out-of-phase load histories could be correlated using Findley's equivalent shear stress model. The in-phase and out-of-phase test data could not be correlated using a maximum principal stress model, but a model based on a von Mises effective stress did better than the former but not as well as Findley's model. The ability of the current fatigue design codes to deal with nonproportional loading cases was evaluated.

ACKNOWLEDGMENTS

This study was conducted in the Materials Engineering Research Laboratory (MERL) of the University of Illinois at Urbana-Champaign. Initial funding was provided by the Edison Welding Institute/Welding Research Council (EWI/WRC), New York, NY and the Fracture Control Program at the University of Illinois at Urbana-Champaign. Additional funding was also provided by the Academy of Finland/National Research Council for Technology (Suomen Akatemia, Teknistieteellinen toimikunta), Ministry of Trade and Industry of Finland (Kauppa- ja teollisuusministeriö) and the Finnish Cultural Foundation (Suomen Kulttuurirahasto).

Professor F. V. Lawrence, Jr., mentor and thesis advisor, is gratefully acknowledged for his initial idea to this investigation, his advice, encouragement and many generous contributions to my personal and professional development. Special thanks are extended to Dr. P. Kurath for his expert assistance in conducting the laboratory experiments, our stimulating discussions both inside and outside of the laboratory and his unflagging and friendly support and patience. Professor D. F. Socie is sincerely thanked for his advice and many stimulating discussions. Professors D. Marriott and H. Sehitoglu are gratefully acknowledged for their guidance and for serving on my doctoral committee. Professor E.J. Niemi from Lappeenranta University of Technology, Finland is specially thanked for his encouragement to pursue academic studies at the University of Illinois and for his kind help throughout my academic career. Professor R. Dodds and his graduate assistants Mr. M. Keppel and Mr. P. Vargas from the Department of Civil Engineering are sincerely thanked for their invaluable help in performing the finite element analyses. Mr. B. Reynolds of the Civil Engineering Machine shop expertly prepared the test specimens for this investigation.

TABLE OF CONTENTS

List of Tables

LIST OF FIGURES

LIST OF SYMBOLS

a	Peterson's material dependent parameter (mm)
b^*, b^{**}	Bending fatigue strength exponent for local principal, von Mises stress
b_0	Torsional fatigue strength exponent for Findley's local equal shear stress
g	Guest's constant
k	Findley's constant
r	Notch root radius (mm)
F	Findley's equivalent nominal shear stress range (MPa)
K_f, K_{fmax}	Fatigue notch factor, maximum fatigue notch factor
K_T	Elastic stress concentration factor
K_{σ_1}	Elastic principal stress concentration factor
K_{ε_1}	Elastic principal strain concentration factor
$K_{\sigma_{eff}}$	Elastic von Mises stress concentration factor
$K_{\varepsilon_{eff}}$	Elastic von Mises strain concentration factor
N_f	Cycles to failure
R_σ, R_τ	Nominal bending, torsional stress ratio
S_i	Nominal principal stress (MPa); i = 1, 2, 3
S_x^{max}	Maximum applied bending stress (MPa)
S_n^{max}	Maximum nominal normal stress (MPa) on maximum shear stress orientation
Γ_{xz}^{max}	Maximum applied torsional stress (MPa)
Γ_n	Guest's equivalent nominal shear stress amplitude (MPa)
α, θ	Orientation angle between specimen axis and the maximum local shear stress amplitude, maximum local principal stress amplitude (degrees)
λ	Nominal bending stress to nominal torsional stress ratio
σ_y	Tensile yield strength (MPa)

σ_U	Ultimate tensile strength (MPa)
σ_H^m	Mean local hydrostatic stress (MPa)
σ_i^m	Local mean stress (MPa); i = x,y,z
$\frac{\Delta\sigma_i}{2}, \frac{\Delta\tau_{ij}}{2}$	Local normal, shear stress amplitude; $i \neq j$, i = x, y, z; j = x, y, z
ΔS_x	Nominal bending stress range (MPa)
ΔS_e	Endurance limit under bending only loading (cycles)
$\Delta\Gamma$	Nominal torsional stress range (MPa)
$\Delta\Gamma_e$	Endurance limit under torsion only loading (cycles)

1. INTRODUCTION

1.1 THE FATIGUE STRENGTH OF WELDMENTS

The fatigue strength of weldments reflects the severity of the local stress concentration at the weld discontinuities inherent in the weldment. Mean stresses and material properties are frequently assumed to have a minimal effect on the fatigue strength of welded joints, since most welded structures are in the as-welded condition and contain welding-induced tensile residual stresses of the order of the yield strength of the material [1, 2 - 5].

Most of the currently employed fatigue design codes for weldments are based on extensive laboratory fatigue tests and group various joint configurations into categories according to their fatigue strength. Fatigue strength is evaluated in terms of the the applied nominal bending stress range [6] or maximum nominal principal stress range [1, 2, 7, 8]. In these fatigue design codes, no experimental data is available to evaluate loading conditions where the applied loads are out-of-phase and nonproportional - a situation that is often encountered in the operating environment of welded structures.

1.2 PROPORTIONAL AND NONPROPORTIONAL FATIGUE LOADING OF WELDMENTS

The extensive experimental data considered in the fatigue design codes are from laboratory tests on uniaxially-loaded, small-scale welded details [9] or from bending tests on nearly full-scale welded girders [10-12]. An example of a conventional three-point bending test with a fixed (stationary) position of the applied load is shown in Fig. 1. In these common laboratory tests, the loading-induced nominal bending and shearing stress components in the vicinity of the web stiffener welds are always in-phase (proportional); in other words, the bending and shearing stresses increase and decrease together resulting in a fixed principal stress direction during a loading cycle.

Unlike the common laboratory mode of loading, the service load of beams frequently involves moving loads. Typical examples are welded highway bridge girders and overhead crane runway beams, which often have stiffeners or other attachments welded onto the webs. These beams and girders sustain moving loads resulting in nominal bending and shearing stress-time histories that are out-of-phase.

An example with a moving point load is illustrated in Fig. 2. The bending and shearing stresses in the vicinity of the center of the span of a simply supported beam

increase proportionally until they reach their maximum values as the idealized point load approaches the location being analyzed; after which, the shearing stress reverses completely while the bending stress remains at its maximum. This shear reversal causes the loading path for the moving point load to be out-of-phase. Finally, after the moving load passes the location being analyzed, both bending and shearing stresses decrease to zero in a proportional manner. It should be noted that the ratio of bending to shear stress amplitudes varies along the span length of a simply-supported beam. This ratio is maximum at the span center and minimum at the location of the supports. Only at the span center is the mean shear stress zero for the reversal of shear when the bending stress is at its maximum. For the loading cases discussed above, the bending stresses were from zero to maximum.

The conventional laboratory bending fatigue tests with a stationary load are commonly employed to simulate the moving loading case. However, the conventional laboratory bending tests do not duplicate exactly the actual structural loading conditions: compare Figs. 1 and 2.

1.3 PREVIOUS STUDIES OF PROPORTIONALLY AND NONPROPORTIONALLY LOADED NOTCHED SPECIMENS

1.3.1 EARLY EMPIRICAL STUDIES

In 1951, Gough, Pollard and Clenshaw [13] conducted the first extensive series of completely reversed in-phase combined bending-torsion fatigue tests for 12 different mild steels. Both unnotched and notched (0.02 in. deep and 55 degree V-notch) specimens were considered. The test materials were chosen to represent a range of the ductile steels employed in aircraft and automobile industries and covered a wide variety of tensile strengths and microstructures. For each material and specimen geometry, various different bending-to-shear stress ratios (λ) were employed: ∞ (bending only), 7.464, 3.464, 2.0, 1.155, 0.536 and 0 (torsion only) in the life regime of $5 \cdot 10^4$ to 10^7 cycles.

$$\lambda = \frac{S_x^{max}}{\Gamma_{xz}^{max}} \tag{1}$$

It was found that an empirical ellipse quadrant relation (Eq. 2) correlated their test data irrespective of the tensile strength, microstructure and heat treatment of the solid and hollow unnotched steel specimens:

$$\left(\frac{\Delta S}{\Delta S_e}\right)^2 + \left(\frac{\Delta \Gamma}{\Delta \Gamma_e}\right)^2 = 1 \tag{2}$$

For the notched steel specimens and unnotched cast iron samples, it was found that an empirical ellipse arc equation (Eq. 3) correlated the test data better:

$$\left(\frac{\Delta \Gamma}{\Delta \Gamma_e}\right)^2 + \left(\frac{\Delta S}{\Delta S_e}\right)^2 \left(\frac{\Delta S_e}{\Delta \Gamma_e} - 1\right) + \frac{\Delta S}{\Delta S_e}\left(2 - \frac{\Delta S_e}{\Delta \Gamma_e}\right) = 1 \tag{3}$$

No physical interpretation was ascribed to Eqs. 2 and 3. Note that if $\frac{\Delta \Gamma_e}{\Delta S_e} = 0.5$, Eq. 3 reduces to Tresca's maximum shear stress criterion, and to maximum principal stress criterion when $\frac{\Delta \Gamma_e}{\Delta S_e} = 1$.

In 1954, Thurston and Field [14] conducted completely reversed in-phase combined bending-torsion fatigue tests for specimens fabricated from seven different ductile steels. The experimental program was a continuation of the project initiated by Gough et al. [13]. The hollow specimens had a cylindrical hole of 1/10 of the 0.42 and 0.5 in. outer diameter which pierced the diameter of the specimens. The ellipse arc relation (Eq. 3) adequately correlated their test data for the notched ductile steel specimens.

In 1956, Findley [15] proposed a modification of the principal stress theory for notched steel specimens under combined bending - torsion:

$$\frac{\Delta S}{\Delta S_e} + \left(\frac{\Delta \Gamma}{\Delta \Gamma_e}\right)^2 = 1 \tag{4}$$

Equation 4 was found to be in good agreement with the available data on notched ductile steels. Findley and Mathur [16, 17] also proposed a modification of the principal shear stress theory corrected for anisotropy, which was shown to be identical to Gough's ellipse quadrant, Eq. 2. It was also shown that the modified principal strain theory, when corrected for anisotropy, is identical to Gough's ellipse arc relation, Eq. 3.

Sines [18, 19] proposed a criterion in 1959 relating the octahedral shear stress amplitude and static hydrostatic stress. It was stated that "for a given fatigue life, the permissible amplitude of the root-mean-square of the shear stresses over all planes is a

linear function of the static normal stresses averaged over all planes". Similarities with Findley's model (Eq. 7) can be observed. Sines' model is identical to Gough's ellipse quadrant (Eq. 2) when the ratio of torsional fatigue limit to bending fatigue limit is 0.577, and identical to von Mises criterion when applied to fully reversed combined bending and torsion [20].

Tipton and Nelson (1989) [21, 22] tested notched shafts manufactured from normalized AISI 1045 steel as a part of the SAE Notched Shaft Program. Fully reversed bending only, torsion only and combined in-phase and 90° out-of-phase bending-torsion fatigue test results were analyzed with the modified shear stress (SALT) and modified octahedral stress (SEQA) criteria of the 1978 ASME Boiler & Pressure Vessel Code, Section III [23] and Code Case N-47-12 of Section III [24], respectively. For in-phase loading, the SALT and SEQA approaches reduce to the Tresca and von Mises criteria, respectively. Both criteria were found to give non-conservative fatigue life predictions with 90° out-of-phase loading.

1.3.2 STUDIES BASED ON PHYSICAL OBSERVATIONS

In 1954, Stulen and Cummings [25] proposed a model similar to Guest's static failure criterion (Eq. 5) [26 - 28] employing the interaction of the ranges of maximum shear stress and normal stress on the maximum shear stress plane:

$$\frac{S_1 - S_3}{2} + g\left(\frac{S_1 + S_3}{2}\right) = \text{constant} \tag{5}$$

where S_1 and S_3 are the maximum values of the largest and smallest nominal principal stresses during a loading cycle. Equation 5 states that constant fatigue lives are a function of the maximum shear stress range modified by the normal stress range on the maximum shear stress plane. The effect of the normal stress is indicated by a material constant g. The theory was tested against available experimental data found from literature covering bending only, torsion only and combined in-phase bending-torsion fatigue tests on smooth and notched, ductile and brittle metals in the life regime of 10^4 to 10^8 cycles. Results were compared with the distortion energy and maximum shear theories and the proposed "critical plane" approach correlated the available data consistently better. It was later shown that the Stulen and Cummings approach reduces to the complete Guest's law (Eq. 6) [21]:

$$\Delta\Gamma_n = \frac{1}{2}\left(\sqrt{\left(\frac{\Delta S}{2}\right)^2 + 4\left(\frac{\Delta\Gamma}{2}\right)^2} + \left(\frac{2\Gamma_e}{S_e} - 1\right)\frac{\Delta S}{2}\right) \tag{6}$$

Guest further noted that Gough's ellipse arc (Eq. 3) for notched steel specimens is equivalent to the "critical plane" criterion (Eq. 6).

Based on physical observations of the orientation of initial fatigue cracks of various steels and aluminum alloys [20], Findley (1956) discussed the influence of the normal stress acting on the maximum shear stress plane [29]. A "critical plane" model was subsequently introduced [30, 31]:

$$\Delta\Gamma^{max} + k\, S_n^{max} = F \tag{7}$$

In other words, the critical alternating shear stress ($\Delta\Gamma^{max}$) decreases with an increase in maximum normal stress (S_n^{max}) on the plane of the critical alternating shear stress from a value F when normal stress is zero. The effect of the normal stress is influenced by a material constant k. The maximum normal stress was formulated as the sum of the normal stresses resulting from the amplitude and mean stresses.

McDiarmid [32] conducted an extensive literature survey on the multiaxial fatigue in the high-cycle regime in 1972. He showed that the ellipse quadrant proposed by Gough et al. (Eq. 2) can be divided into components of maximum shear stress amplitude and the normal stress amplitude acting on the plane of maximum shear stress amplitude - a model similar to that of Findley (Eq. 7) [30, 31]. McDiarmid also argued that his proposed model is based on physical observations on the effect of normal stress on the maximum shear stress orientation; whereas, the Gough ellipse arc and ellipse quadrant were purely empirical.

In 1976, Grubisic and Simbürger [33] conducted combined in-phase and out-of-phase bending-torsion fatigue tests on fillet notched 0.44% carbon steel specimens in the life regime of $2 \cdot 10^4$ to $3 \cdot 10^5$ cycles and $\lambda = 1.74$. An "effective straining" model was proposed which requires the examination of all planes in a three-dimensional body for the most unfavorable combination of shear and normal stresses. It was experimentally observed that out-of-phase loading was more damaging than in-phase loading, a feature also reflected by their theoretical model.

In 1985, Lee [20] tested smooth cantilever specimens fabricated from SM45C structural steel (equivalent to SAE 1045) under constant amplitude, fully reversed in-phase and 90° out-of-phase combined bending-torsion in the life regime of 10^4 to 10^6 cycles with the bending-to shearing stress ratios (λ) varying between 0.79 - 5.35. Lee's proposed model was based on Gough's ellipse quadrant relation (Eq. 2), which was further modified to account for the phase difference and material via an empirical constant. The theory was tested against a wide range of available experimental data including notched specimens. Fatigue life predictions with the proposed model agreed significantly better than those of the 1978 ASME approach [23, 24] and predicted published biaxial experimental data for various steels quite well.

In 1985, Fash, Socie and McDowell [34] conducted combined in-phase bending-torsion fatigue tests on normalized 1045 notched shafts in the life regime of 10^3 to 10^6 cycles (λ = 0, 0.27 to 1.4, ∞). Three-dimensional elastic-plastic finite element analysis was carried out to capture local strain components at the critical region of the notch. Test results were evaluated by using three commonly employed extensions of static yield criteria as fatigue damage parameters:

i) maximum principal strain,
ii) effective strain (von Mises) and
iii) maximum shear strain (Tresca).

Additionally, two strain-based "critical plane" approaches were also evaluated: the Lohr-Ellison and the Kandil-Brown-Miller models. An order of magnitude difference between experimental and predicted fatigue lives was observed for each of the five fatigue theories.

A common theme in the above studies is that the data has been represented in terms of the purely empirical ellipse quadrant interaction equation (Eq 2). This interaction equation can be split into the maximum shear stress and corresponding normal stress components, which quantities closely reflect the driving forces for fatigue damage in ductile steels. Consequently, approaches based on the maximum shear stress and corresponding normal stress components should lead to better correlations with the fatigue data.

1.4 Previous Studies of Proportionally and Nonproportionally Loaded Welded Members

Most published work on the effects of moving loads on the fatigue of weldments have been concerned with longitudinal fatigue cracking of upper web-to-flange welds and web stiffener welds in crane-runway girders due to cyclic, Herzian wheel pressure distribution [35 - 41] or on the effects of dynamic deflections as a result of moving traffic loads in highway bridge beams [42, 43]. Although the nonproportional biaxial loading situations have been acknowledged [11, 44], there is no published work about the above-mentioned out-of-phase loading simulations that occur in structures sustaining moving loads [45 - 47]. The lack of laboratory test data has mainly been due to experimental difficulties in duplicating realistic out-of-phase multiaxial loading situations. Only during the past 30 years have the laboratory test equipment been developed to conduct complex multiaxial cyclic out-of-phase laboratory experiments - most of which, however, have been conducted in the low-cycle regime [48 - 52].

In 1959, Kouba and Stallmeyer [53] studied the flexural fatigue behavior of nearly full-scale beams with various web stiffener configurations using test specimens fabricated from ASTM A373-54T steel. Specimens were fatigue tested with stationary applied loads under constant amplitude four-point bending loading ($R_\sigma = 0$) in the life regime of $5 \cdot 10^5$ to $6 \cdot 10^6$ cycles. Most failures took place outside of the region of pure bending moment distribution, suggesting that shear stresses should be considered in the analysis. The bending-to-shear stress ratios (λ) in the failure locations ranged from 0.19 to 1.25. It was found that the test data correlated much better with nominal principal stress range than with maximum applied bending stress range. The observed crack orientations also agreed with predicted principal stress directions.

In 1962, Munse and Stallmeyer [54] conducted studies on the effect of web stiffener welds to the fatigue capacity of near full-scale welded highway bridge girders and summarized the work done at the University of Illinois. Test specimens fabricated from ASTM A373 and ASTM A7 steels were tested under similar four-point bending loading conditions. Bending-to-shear stress ratio (λ) ranged between 0.19 and 1.25 Most failures took place at stiffeners located at the moment gradient region where there are shear stresses present. The best correlation of the test data was obtained employing nominal principal stress range at the crack initiation location (nominal shear stresses included) rather than applied flexural (bending) stress alone. It was found that when the web stiffeners are not

welded to the tension flange, the shear stresses in the web should be included in design applications involving bridge beams subjected to flexural cyclic stresses.

Moyar and Garg [17, 55] later (1983) re-analyzed some of the Munse and Stallmeyer data with regard to the fatigue damage parameter. They calculated the nominal stresses at the failure location and correlated the data with maximum nominal principal stress range, maximum shear stress range (Tresca), and maximum octahedral shear stress range (von Mises). Both of the shear stress-based approaches provided better data correlation than the principal stress approach in the high-cycle regime.

In 1962, Gurney and Woodley [56] tested near full-scale structural steel specimens fabricated from BS 968 steel having BS 15 mild steel stiffeners welded onto the web both in the moment gradient and constant moment sections. Fatigue tests were carried out under constant amplitude four-point bending ($R_\sigma = 0$) in the life regime of $5 \cdot 10^5$ to $5 \cdot 10^6$ cycles. The bending-to-shear stress ratios (λ) ranged from 0.44 to 1.33. It was concluded that the test data correlated well with the maximum principal stress range with regard to the prediction of fatigue life and cracking direction.

During the 1970's, Fisher at al. conducted a literature survey and similar laboratory experiments in order to develop mathematical design relationships that could define the fatigue strength of steel beams with statistical confidence [10] and to study the effects of web stiffeners to the fatigue characteristics of bridge beams [11]. Test specimens fabricated from ASTM A36, A514 and A441 steels were fatigue tested under constant amplitude, stationary four-point bending loading ($R_\sigma = 0$) in the life regime of 10^5 to 10^7 cycles. The bending-to-shear stress ratios (λ) varied between 3.23 and 4.55. On the basis of their experimental results, they argued that the bending-to-shear stress ratios in previous studies [53, 56] were too low for bridge beam applications, because typical highway bridge beams are so heavily biased towards bending ($\lambda > 1.67$) that the effects of shear could be totally ignored in designing welded web stiffener welds against fatigue. They concluded that principal stress range and its direction are not significant for purposes of design in stiffened bridge members, even though principal stress range provides the best theoretical correlation of the data. Although the out-of-phase biaxial loading situation in real bridge details was acknowledged, not enough experimental evidence was available to ascertain the significance of rotating principal stresses. Instead, it was recommended that only the nominal applied bending stress range should be used for the fatigue design of the details. These extensive fatigue tests partially form the basis of the current AASHTO fatigue design rules for welded highway bridge beams with stiffeners [6, 57].

In 1986, Yung and Lawrence [58] designed a tube-to-plate girth-welded specimen geometry fabricated from ASTM A519 cold-drawn seamless steel tube and A36 hot-rolled steel plate and conducted bending only, torsion only and in-phase combined bending-torsion fatigue tests. The experimental bending-to-shear stress ratios (λ) employed were ∞ (bending only), 2.88, 2.0, 1.75, and 0 (torsion only) and the laboratory fatigue lives ranged between 10^4 - 10^6 cycles. The experimental data was correlated using the amplitudes of bending stress, octahedral shear stress (von Mises) and maximum principal stress. Again, better correlation of the test data was obtained when the shear stresses were included in the analysis, as both the principal and octahedral shear stress models do this.

Common to all of the above studies is that the loading was applied in-phase, resulting in fixed principal stress directions. Macroscopic cracking orientation was always observed to occur perpendicular to the maximum nominal principal stress range. The proportional and in-phase laboratory fatigue tests of these types form the basis of the widely accepted nominal principal stress range philosophy in current design practice [3 - 5].

The only published work on nonproportional biaxial fatigue tests on welded details known is by Archer in 1987 [59]. Rectangular hollow section beams made of BS4360 grade 43C steel with welded BS4360 grade 43A steel attachments were subjected to various combinations of bending and shearing stresses, Fig. 3. The phase difference was produced by varying the frequency of the applied loads. The data was analyzed with Gough's ellipse quadrant (Eq. 2), Findley's modified principal stress theory (Eq. 5) and a cubic form of (Eq. 2). The results were then compared to the BS5400 class F mean fatigue design curve [1]. The analysis with the available limited experimental data suggested no pronounced difference between proportional and nonproportional loading.

In summary, very little information exists regarding the influence of out-of-phase loading on the high-cycle fatigue of weldments. Most published data on the fatigue of welded joints are based on laboratory fatigue tests, where the applied loading is proportional and in-phase resulting in fixed principal stress directions. However, as the location of the applied loading moves in time (as in highway bridge beams, overhead crane box beams etc.), the principal stress directions rotate. Laboratory simulations with nearly full scale beams subjected to moving point loads are complex and expensive, so little experimental work has been done to evaluate the fatigue characteristics of web stiffener weldments subjected to nonproportional loadings.

1.5 PURPOSE AND SCOPE

The proportional and nonproportional high-cycle fatigue behavior of mild-steel, tube-to-plate welded specimens was studied. In-phase bending and torsion constant amplitude fatigue tests were used to define the weldment (HAZ) baseline material properties and also to serve as a comparison with out-of-phase tests.

This entire work is predicated on the assumption that the cyclic stress state in a tube-to-plate weldment subjected to bending and torsion can replicate the stress state at critical locations in large-scale structures and, hence, that tests on these laboratory specimens can elucidate the effect of nonproportional loading on structures in service (Fig. 4). Thus, out-of-phase combined bending-torsion loading paths were generated for a tube-to-plate specimen to simulate cyclic stress states typical of highway bridge beams subjected to a single passage of a vehicle. In-phase, combined bending-torsion experiments were conducted on the tube-to-plate specimen to simulate the common laboratory tests involving stationary loads on a beam.

The fatigue test results were correlated with various multiaxial fatigue damage parameters based on the local, notch-root stresses from finite element analyses of the weld-toe notches. The reliability of the current fatigue design codes in dealing with nonproportional loading cases was evaluated.

2. EXPERIMENTAL PROGRAM

2.1 MATERIALS AND SPECIMEN FABRICATION

The materials employed were seamless, cold-drawn steel tubing meeting the ASTM A519 standard and hot-rolled steel flat plate meeting the ASTM A36 standard. Tube-to-plate weldments having the geometry and dimensions shown in Fig. 5 were fabricated. The mechanical properties for these two steels are given in Table 1. The microstructure and microhardness of the welded joint are shown in Figs. 6 and 7, respectively. Identical materials and similar specimen geometry were also employed in an earlier study by Yung and Lawrence [58]. The advantage of the small-scale, tube-to-plate geometry employed is the ease and low specimen cost for investigation cyclic out-of-phase stress states.

The only restraint applied during welding was two tack welds, which were used to position the plate in the tube. Welding was carried out in the flat position (tube axis in the vertical position) using a single pass and an automated GMAW-process (MIG) operated at approximately 28 volts and 180 amperes with an average heat input of 18.7 kJ/cm (average welding speed of 2.7 mm/sec) and under 98% Ar - 2% O shielding gas. The solid, filler metal wire of 0.89 mm (0.035 in.) diameter conformed to the AWS E70S-2 standard. All specimens were stress-relieved at 550° C for 2 hours before testing to eliminate residual stresses. Residual stress measurements carried out using X-ray diffraction methods for as-welded and stress-relieved specimens [60, 61] are summarized in Table 2. Similar results were reported earlier for a similar geometry [58]. The location of the X-ray diffraction measurements was less than 3 mm away from the weld toe and is shown in Fig. 4.

2.2 TESTING FACILITY

The servo-hydraulic testing system employed in this study was initially designed for the multiaxial notched shaft fatigue test program of the Society of Automotive Engineers (SAE) Fatigue Design and Evaluation Committee [62]. A schematic of the test system is shown in Fig. 8. The test system capacities for the tube-to-plate welded specimen are 7.3 kNm for bending and 8.1 kNm for torsion. All fatigue tests on the tube-to-plate weldments were conducted under load control using constant amplitude bending, torsion and combined bending-torsion.

The short end of the test specimen was clamped between two machined steel blocks as a cantilever beam (Fig. 8). Additional rigidity was provided by constraining the plate

tightly against the two steel blocks with four additional bolts. Care was taken in ensuring that every specimen was mounted in the same way with regard to bolt torque and tightening order of the bolts. The loading fixture, through which the actuator loads were transferred to the test specimen, consisted of a collet-yoke arrangement. A mono-ball hinge joint was employed to connect the actuators to the base plate of the test frame. Spherical strut ends were employed to mount the actuators and load cells to the specimen loading fixture.

For all $R_\sigma = 0$ tests, the orientation of the test specimen was such that the girth weld "start and stop" position was always at the bottom position (compressive loads). Fatigue crack initiation and subsequent growth occurred at the top position of the weld toe (maximum tensile principal stress location). For completely reversed bending only tests, ($R_\sigma = -1$), the weld "start and stop" position was at the neutral axis. This minimized data scatter resulting from the possible random location of flaws due to weld start and stops. Because of the rotational symmetry of the specimen, the effect of the "start and stop" position of the weld could not be avoided for torsion only loading. The applied bending and torsional moments were calculated from nominal stresses in the vicinity of the weld toe as outlined in Appendix A.

With an analog function generator and signal inverter, any in-phase combination of bending and torsion could be applied by adjusting the amplitude and phase of the two independent hydraulic actuators. Computer control was necessary for the nonproportional out-of-phase loading path simulations. Static and dynamic strain responses were monitored using strain gages attached to the surface of the tube for a few specimens to ensure that the manual and computer controls produced the desired loadings.

2.3 Loading Path Determination

Both proportional and nonproportional loading paths were considered in this investigation. In order to simulate service loadings for the combined bending and torsion tests, it was necessary to determine realistic bending stress/torsional stress ratios. A 310 kN moving load on a bridge beam with a 12.2 m span [63 - 66] was used to calculate representative bending and shearing stresses at various locations in the web-flange intersection of a typical 30-WF-124 bridge beam, as shown in Appendix B. Bending to shear stress ratios (λ) of ∞ (bending only), 7.34, 2.39, 1 and 0 (torsion only) were used for in-phase testing. Previous biaxial research has shown that mean shear stresses have little influence on fatigue damage [26, 27]. Therefore, the ratio of 2.39 was employed for the out-of-phase combined bending-torsion tests (see Appendix B). Loading paths

employed in this study and the experimental results are summarized in Fig. 9 and Table 3, respectively.

3. ANALYSIS AND TEST RESULTS

3.1 FINITE ELEMENT ANALYSES

Three-dimensional finite element (FE) models of the specimen geometry were generated with the software package PATRAN-G, release 2.3 [67]. Twenty-node isoparametric elements were used throughout both models with two elements through the wall thickness in the remote regions of the models (Fig. 10). The coarse element mesh in the remote regions was used to transfer the applied bending and torsional loads from the free end of the tube to the weld toe region. The element mesh was the densest at the location A (Fig. 10), where the maximum stresses for bending only and combined bending-torsion loadings were expected (for torsional only loading, the maximum local stresses remain constant along the circumference of the weld toe). At the location A, there were 8 elements along the global x-direction of the notch surface. The 0.025 mm gap on the root side of the weld between the plate and tube was accurately modeled: see Fig. 10.

The following boundary conditions were applied to the two FE models to mirror the test frame boundary conditions (Sect. 2.2): All skin nodes on the short end of the tube were displacement-constrained in the global x-y-z - directions. Those skin nodes on the plate which were on the unwelded side of the plate and below the bending neutral axis of the specimen were displacement-constrained in the global x - direction. The plate nodes that were within the four bolt hole regions of the plate (Fig. 5) were also displacement-constrained in the global x-y-z - direction. With these boundary conditions, the FE analysis results coincided with experimental strain gage measurements in the global x-direction (approximately 5 mm away from the weld toe) to within 10% for the bending only loading case. For torsion-only loading case, the experimental strain measurements from rosette strain gage also agreed to within 10% with the FE calculations.

The smallest and largest experimentally observed weld toe radii on the tube side of the weld were approximately 0.18 mm and 4 mm in radius, respectively. Weld toe radii suggested in the literature were in agreement with these measurements [68 - 72]. Although the continuous undercut around the tube represents an extreme case, similar observations have also been reported to occur in other welded joints [72, 73]. The "worst case" notch concepts of Lawrence et al. [74] (from Eqns. 12 and 13) would suggest a similar notch radius ($r = a = 0.18$ mm) for the tube material.

Thus two FE models were created to model the weld. Both had weld toes with a continuous undercut of a depth equal to the undercut radius (0.18 mm and 4.0 mm, see Fig. 10). The weld angle was modeled as 45°; the actual measured weld toe angles varied between 30 - 60°. Three different loading cases were analyzed: a) bending only, b) torsion only and c) combined bending and torsion. Local stresses and strains were extrapolated from 3x3x3 integration points to obtain nodal values for each element; element nodal values were then averaged with neighboring elements. ABAQUS structural analysis code [75] was employed in these FE analyses.

Since the FE analysis was linear elastic, all local stress components were proportional to the nominal loading, and all local stresses and strains could easily be evaluated from one FE analysis for a given loading path. The combined loading case was performed to verify the expected applicability of superposition as a technique for the evaluation of combined loading cases. Superposition of bending only and torsion only results coincided with the combined bending and torsion finite element analysis. Due to the subsequent choice of fatigue damage parameters, nodal values with maximum principal stress, maximum von Mises effective stress, and Findley's equivalent shear stress on the maximum shear stress plane were of primary interest.

The stress state below the surface of the notch is somewhat different than that on the surface. Specifically, all six local stress components exist below the surface of the notch, while on the surface the stress state is biaxial. Since fatigue crack initiation from discontinuities may govern the total fatigue life at long lives and since those fatigue cracks that grow into the bulk of material are deemed critical, the local stress states just ahead of the notch tip were of interest. Therefore, the local stress and strain quantities in the subsequent analyses consider a critical location approximately 0.2 mm below the surface of the notch (i.e. at the integration points).

For all loadings, the nodal values were obtained from integration points of the element located at the root of the 0.18 mm and 4.0 mm notches. Tables 4 and 5 summarize the maximum principal stress and strain concentration factors, K_{σ_1} and K_{ε_1} and von Mises' effective stress and strain concentration factors, $K_{\sigma_{eff}}$, and $K_{\varepsilon_{eff}}$ obtained from FE analyses. In the above stress and strain concentration factors, the following definitions were employed:

K_{σ_1} , K_{ε_1} = ratio of maximum local principal stress (strain) to the nominal principal stress (strain),

$K_{\sigma_{eff}}$, $K_{\varepsilon_{eff}}$ = ratio of maximum local von Mises stress (strain) to the nominal von Mises stress (strain).

The maximum local stresses and strains were obtained from the FE analysis, while the maximum nominal stresses and strains were obtained for the corresponding location from the theory of elasticity for a smooth cantilever beam subjected to identical nominal loading.

Once the local stresses and strains at the critical location below the surface of the weld toe were determined from the FE analyses, the local stress history characteristics between in-phase and out-of-phase loading cases subjected to identical maximum nominal loading levels could be compared.

3.2 STRESS HISTORY CHARACTERISTICS FOR IN-PHASE AND OUT-OF-PHASE LOADING

The differences between in-phase and out-of-phase loading for the nominal stress states are documented in [76]. When local stress states are employed in these comparisons, it is imperative to understand the differences in the stress states between torsion and bending. Figure 11a illustrates the torsion only loading results obtained for the local stresses via finite element analysis. The maximum local shear stress is proportional to the difference between maximum and minimum local principal stresses (i.e. Tresca) for this stress state. The two local principal stresses are equal in magnitude but of opposite sign, while the third principal stress is always zero. There is a constant difference between nominal and local stress states for torsion only loading. For torsion-only loading, there is no volume change; and therefore, no constraint condition results from the notch. The shaded circles in Fig. 11a represent the surface plane of the notch.

For bending-only loading (Fig. 11b), such an analogy between the local and nominal stress states does not exist. During the loading cycle, Mohr's local stress circles expand and translate to the position shown for the maximum loads in Fig. 11b. Due to the volume change in bending only loading, severe local constraint conditions are introduced at the notch root. All three principal stresses were non-zero in the finite element analysis;

thus, the determination of maximum local shear stresses with only a knowledge of the maximum principal stress concentration factor (K_{σ_1}) is impossible.

In many metals, slip or shear is assumed to dictate yield, fatigue, and and even static failure. Since notch constraint reduces the the shear stresses and strains, many phenomena, such as notch strengthening and the fatigue notch factor (K_f) being lower than the theoretical notch factor, (K_{σ_1}) can be explained with this observation. In order to quantify the local notch constraint condition for a given loading and specimen geometry and further evaluate any fatigue damage parameter, it becomes necessary to employ three-dimensional analyses.

3.2.1 IN-PHASE COMBINED BENDING-TORSION LOADING

Similar generalized results for the in-phase combined bending-torsion loading are shown in Fig. 12a. At point A, there are no external loads applied and Mohr's circle of stress corresponds to a point at the origin as shown in Fig. 12b. As the applied bending and torsional loads start to increase proportionally and in-phase towards point B, the three local elastic principal stresses and the corresponding maximum local elastic shear stress orientations remain fixed with regard to the specimen axes.

Due to the torsional component of loading, the maximum principal stress orientation and specimen axis (bold solid line) do not coincide. Again Mohr's circles of stress expand and translate in the three-dimensional stress space. At point B, both bending and torsional stresses have reached their maximum local values. The corresponding Mohr's circle of stress for point B is shown in Fig. 12b. Then, both bending and torsion decrease proportionally and in-phase back to zero corresponding to point A in Fig. 12b. Again, the shaded circle represents the surface plane of the notch. The orientation of the maximum principal stress amplitude is at angle (θ) from the longitudinal specimen axis where there is no shear.

There are normal and shearing stresses on all other orientations with respect to the specimen axis (bold solid line). Since Mohr's representation describes only instantaneous local stress states during cyclic loading, the local normal and shearing stress time-histories in various orientations in the notch plane for the in-phase loading path (A - B - A) are shown in Figs. 12c, d and e (longitudinal, maximum local principal stress and maximum local shear stress orientations, respectively).

3.2.2 OUT-OF-PHASE COMBINED BENDING-TORSION LOADING

For comparison, results for a nonproportional out-of-phase combined bending-torsion test (Path I) with identical maximum nominal bending and shear stresses as the combined in-phase test is shown in Fig. 13a. At point A', there are no external loads applied. Again, Mohr's circle of stress is a point in the origin shown in Fig. 13b. As the bending and torsion start to increase towards point B', the change in Mohr's circles mirrors that for the combined in-phase test. At point B', both bending and torsion have reached their maximum nominal values (Fig. 13b). During the following loading path segment (B' - C' - D') the bending stress remains constant, while the torsional stress reverses completely.

Mohr's circles of stress corresponding to the points C' and D' and their relation to the longitudinal specimen axis (bold solid line) are shown in Fig. 13b. This segment of loading causes the out-of-phase nature of the loading cycle, during which the three mutually orthogonal local principal stresses and maximum local shear stresses rotate relative to the longitudinal specimen axis. Finally, both bending and torsion decrease proportionally and in-phase from point D' back to zero corresponding to point A'. The maximum local principal stress amplitudes remain identical between these in-phase and out-of-phase tests. However, there is a shear stress cycle on the maximum local principal stress orientation for the out-of-phase loading. Also, the stress normal to the maximum shear stress plane changes in comparison to the in-phase loading.

For comparison to the in-phase loading cycle, the local normal and shearing stress time histories in longitudinal, maximum local principal stress and maximum local shear stress orientations in the notch plane for the out-of-phase loading path (A' - B' - C' - D' - A') are shown in Figs. 13c, d and e, respectively.

While the maximum local principal stress amplitudes remain identical to these two loading paths, there are shear stresses on the maximum principal stress orientation for the out-of-phase loading. In general, the evaluation of the stress histories on all orientations is required to determine the maximum amplitude of a given stress parameter for the out-of-phase loading. In this investigation, only the stress states on the plane of the notch surface were of interest and corresponded to the cracking observations.

3.3 LOCAL STRESS-BASED FATIGUE DAMAGE PARAMETERS

Since the local stress time-histories at various orientations between in-phase and out-of-phase loading cases were different, it is important to study whether these differences affect the experimental fatigue life and fatigue life prediction. Good results were obtained in early work [76] using remote stresses . In the current study, only local stresses at the critical location below the surface of the notch were considered to obtain greater prediction accuracy and to allow the comparison of different weld geometries.

3.3.1 MAXIMUM PRINCIPAL STRESS AMPLITUDE

The local stress components were evaluated from the linear elastic finite element analysis below the surface of the root of the r = 0.18 mm notch. These local stress components were utilized to determine the local principal stress magnitudes by solving the roots of the cubic equation involving the stress invariants of the stress tensor. In the fatigue analysis, it was assumed that only the maximum local principal stress amplitude modified by Morrow's mean stress correction [77] dictates fatigue damage. Together with a Basquin-type life equation [78] the following format was employed:

$$\frac{\Delta \overset{\bullet}{\sigma}_1}{2} = \frac{\Delta\sigma_1^{max}}{2}\left[1 - \frac{\sigma_1^m}{\sigma_f^*}\right] = \left[1 - \frac{\sigma_1^m}{\sigma_f^*}\right]\sigma_f^*(N_f)^{b^*} \qquad (7)$$

Constants σ_f^* and b^* (Fig. 14) were determined from completely reversed bending only tests where no mean stresses are present. For other loading cases, the mean stresses were assumed to be the mean, local, principal stresses and that they do not relax. Results for this analysis are shown in Fig. 14. An order of magnitude difference in life was experimentally observed for in-phase and out-of-phase loading for which this parameter predicts equal fatigue damage.

3.3.2 VON MISES EFFECTIVE STRESS AMPLITUDE

A traditional design approach has been to extend the use of classical multiaxial yield criteria as multiaxial stress-based fatigue theories. The most common of these theories are the maximum shear stress (Tresca) and the octahedral shear stress (von Mises). Elastic local stress components from finite element analysis were employed in the von Mises effective stress formulation. Von Mises effective local stress amplitude combined with

Morrow's mean stress correction and Basquin's life relation was utilized to evaluate fatigue damage:

$$\frac{\Delta \dot{\sigma}_{eff}}{2} = \frac{\Delta\sigma_{eff}^{max}}{2}\left[1 - \frac{\sigma_{eff}^{m}}{\sigma_f^{**}}\right] = \left[1 - \frac{\sigma_{eff}^{m}}{\sigma_f^{**}}\right]\sigma_f^{**}(N_f)^{b^{**}} \tag{8}$$

with

$$\frac{\Delta\sigma_{eff}}{2} = \frac{1}{\sqrt{2}}\left(\left(\frac{\Delta\sigma_x}{2} - \frac{\Delta\sigma_y}{2}\right)^2 + \left(\frac{\Delta\sigma_x}{2} - \frac{\Delta\sigma_z}{2}\right)^2 + \left(\frac{\Delta\sigma_y}{2} - \frac{\Delta\sigma_z}{2}\right)^2 + \ldots\right)$$

$$\left(\ldots + 6\left\{\left(\frac{\Delta\tau_{xy}}{2}\right)^2 + \left(\frac{\Delta\tau_{xz}}{2}\right)^2 + \left(\frac{\Delta\tau_{yz}}{2}\right)^2\right\}\right)^{0.5} \tag{9}$$

and

$$\sigma_H^m = \frac{\sigma_x^m + \sigma_y^m + \sigma_z^m}{3} \tag{10}$$

Constants σ_f^{**} and b^{**} (Fig. 15) were again determined from completely reversed bending only tests. The mean stresses were assumed to be the mean local hydrostatic stresses (Eq. 10) and that they do not relax. Since von Mises stress is a scalar quantity, it is difficult to represent the rotation of principal stress axes for the out-of-phase loading. Therefore, for this analysis, the local stress amplitudes (Eq. 9) have been employed even for the out-of-phase loading cases. Mean stress has also been formulated as a hydrostatic stress utilizing the local mean stress components. The results shown in Fig. 15 again incorporate a Morrow format mean stress correction. This method could be considered as a shear-based theory even though the nomenclature in Eq. (9) is used to compare multiaxial loading to uniaxial data.

3.3.3 Findley Equivalent Shear Stress Amplitude

Fatigue cracks formed on the plane of the maximum shear stress in the majority of tests. It has also been reported that the formation of fatigue cracks in welds originates from slip bands [79], suggesting that a shear-based approach might characterize the fatigue mechanisms in welded joints. More recent approaches give a physical interpretation of the damage process by identifying cracking orientations. Findley's approach [24, 25] is an

alternate shear-based model. The analysis employs the local maximum shear stress amplitude on the plane of maximum shear together with the corresponding local normal stress on that plane. The following form for an equivalent maximum shear stress was suggested for high-cycle fatigue [80]:

$$\frac{\Delta \overset{\bullet}{\tau}}{2} = \frac{\Delta \tau_{max}}{2} + k\,\sigma_n^{max} = \tau_f^*\left(N_f\right)^{b_0} \tag{11}$$

with

$$\sigma_n^{max} = \frac{\Delta \sigma_n}{2} + \sigma_n^{mean} \tag{12}$$

The constants τ_f^* and b_0 reported in Fig. 16 were determined from torsion only tests, where the normal stress is zero on the maximum shear orientation. The maximum local shear stress amplitude on the plane of the notch surface and the corresponding local normal stress amplitude were evaluated from the finite element analysis results as described earlier. The influence of the maximum normal stress is indicated by the material constant (k). The constant (k) was determined by comparing bending only and torsion only tests by varying (k) until the best correlation coefficient between equivalent maximum local shear stress amplitude versus cycles to failures was obtained. With the assumption that the local mean normal stress relaxed completely (i.e. $\sigma_n^{mean} = 0$) very early in life, a value of k = 0.24 results. This value is similar to the k = 0.3 value reported by Findley for structural steel [24]. Results for this fatigue damage parameter are shown in Fig. 16. The best overall correlation is obtained utilizing this approach.

4. DISCUSSION

4.1 FATIGUE LIFE ESTIMATION

Three fatigue damage models were compared based on **local** (notch root) stresses determined from the (r= 0.18 mm) FEM analyses:

- The first model was based on maximum local principal stresses.
- The second model was based on the local von Mises effective stress.
- The third model was based on Findley's local equivalent shear stress.

The following criteria were utilized to evaluate and compare the fatigue damage models: 1) How well does a fatigue damage parameter quantify the in-phase data; and, 2) Does an equal value of the damage parameter result in similar experimental lives for in-phase and out-of-phase loading? Run-out tests were ignored for these comparisons.

The experimental loading paths F, I and J with identical maximum load levels (specimens 9, 11, 12, 13, 102, 103, 104, 6, 10, 16 and 100, Table 3) were used to compare the three damage formulations. Experimentally an order of magnitude reduction in fatigue life was observed for loading path I in comparison to F. Path J lives were halfway between I and F.

In summary, the local principal stress model predicted identical fatigue lives for all three loading paths. The local von Mises approach predicted identical fatigue lives for loading paths F and J, while predicting an increased fatigue damage for loading path I. Only the Findley model predicted the experimentally observed trend that loading path I was more damaging than J, which was more damaging than F (Fig. 17). The experience with each of the three damage parameters is discussed in more detail below:

4.1.1 MAXIMUM PRINCIPAL STRESS AMPLITUDE

Considering the maximum local principal stress amplitude with Morrow's mean stress correction as the fatigue damage parameter, even the torsion only test data is not adequately characterized by this method of analysis (Fig. 14). Fatigue damage for torsion only loading was underestimated by up to two orders of magnitude in comparison to the baseline completely reversed bending only data. The in-phase combined loading data were correlated to within a factor of three to the baseline data, but these tests had a definite bias towards bending. Since simple in-phase data could not be characterized, the inability to

predict out-of-phase loadings is not surprising. Comparing fully reversed ($R_\sigma = -1$) and $R_\sigma = 0$ bending only data in Table 3 indicates that load ratio or mean stress has a minimal effect for the range of fatigue lives under consideration.

A similar degree of correlation results if mean local principal stresses are completely ignored in the analysis indicating that the fatigue damage parameter is also rather insensitive to mean stresses.

This method cannot be formulated to account for the local notch constraint resulting from the bending component of loading for this specimen. Consideration of a maximum principal local strain-based approach would further emphasize the trends evidenced for the stress analysis. The ratio of bending to torsional stress concentration factors (Table 4) are 1.66 for stress and 2.55 for strain. Hence, a large deviation of the torsional loading would result if bending were used as a baseline. Utilizing Peterson's empirical relation (Eqns. 13 and 14) [81] and setting r = a to obtain a stress based K_{fmax} for bending (3.04) and torsion (2.53) results in a ratio of 1.20[1] .

$$K_f = 1 + \frac{K_T - 1}{1 + \frac{a}{r}} \tag{13}$$

$$a \approx 2.54 \cdot 10^{-2}\left(\frac{2070}{S_U}\right)^{1.8} \tag{14}$$

4.1.2 VON MISES EFFECTIVE STRESS AMPLITUDE

Using the von Mises effective local stress amplitude to correlate the test data, long-life torsion test data were a factor of four longer than the completely reversed bending baseline data. In-phase combined bending and torsion test data were correlated within a factor of four. Overall trends indicate an overestimation of fatigue damage, inferring a conservative design criterion. The out-of-phase test data correlation with the baseline data improved in comparison to the local principal stress amplitude. Overall, the test data was correlated within a factor of four (Fig. 15).

---

[1] The application of the above K_f concept would tend to improve the correlation of the data. However, this method artificially accounts for notch constraint, and does not model the actual fatigue damage phenomenon.

Again, ignoring the local mean hydrostatic stresses results in similar data correlation as with mean stresses. Since the von Mises effective stress amplitude is proportional to the octahedral shear stress amplitude, this parameter can also be viewed as a shear-based approach. With this interpretation, the fact that this damage parameter predicts the nonproportional test data slightly better than the local principal stress amplitude could be attributed to the shear-based nature of this approach. Being a scalar quantity, this model does not give any interpretation for the fatigue damage orientation, hence the cracking observations will render little insight as to the appropriateness of this analysis technique. Moreover, the local stress components are often out-of-phase, which feature is not accounted for with this method of analysis. However, the technique does account for notch constraint because it is based on the FE - analysis of the notch root stress state.

Since the ratio of bending to torsional effective stress concentration factors are similar for stress and strain (Tables 4 and 5), consideration of a strain-based approach would not qualitatively alter the trends evidenced for the stress analysis.

4.1.3 Findley's Equivalent Shear Stress Amplitude

In Findley's equivalent shear stress amplitude model, the local mean normal stresses on the plane of maximum shear stress amplitude were assumed to relax early in life, and they were thus ignored in the analysis.[1] It should be noted that this analysis was the most sensitive to mean stresses. The baseline in-phase torsion only data at long lives ($N_f > 10^5$ cycles) correlated with the Findley model to within a factor of two (Fig. 16). This result is anticipated since both in-phase torsion and bending were used to fit the baseline material constants. The largest deviation occurs in the short-life region where the elastic assumptions of the current analysis are somewhat inappropriate. The observation that run-out tests generally fall below the baseline data is encouraging. Experimentally

---

[1] Since the normal stress contributed significantly to the fatigue damage assessment with the Findley model, the deformation characteristics were further studied for loading paths G and I (Table 3). Some experiments were conducted with smooth tubular specimens manufactured from the tube material under tension-torsion strain control to study the mean normal stress behavior of these two non-proportional loadings. The maximum shear stress orientation is perpendicular to the specimen axis for these two loading paths, hence the normal stress is in the axial direction of the specimen. Mean axial loads (stresses) were found to relax close to zero levels very early in life for both nonproportional loading cases. If one considers the local notch behavior to be strain-controlled, one could infer that the mean stresses in the tube-to-plate specimen would also relax. Hence, only the normal stress amplitude term of Eq. (11) remained effective. It is important to note that there there is no normal stress amplitude on the maximum shear stress orientation for loading paths G and H.

observed differences between in-phase and out-of-phase stress histories are reflected by this model. Slightly non-conservative life estimates result for the out-of-phase loading. Correlation of the data for all loading paths is within a factor of three.

Ignoring aforementioned mean stress phenomena would marginally affect the previous two analyses (Sections 3.3.1 and 3.3.2), but improve data correlation to within a factor of three for Findley's analysis. Since the scatter in experimental data between identical in-phase and out-of-phase tests was within a factor of two, further improvements in the correlation of this data are unlikely. A conceptually similar strain-based approach has been proposed by Kurath and Fatemi [82] and verified for 1045 steel subjected to similar loading.

4.2 SURFACE CRACKING OBSERVATIONS

The macroscopic orientation of fatigue crack initiation was confined either to the weld toe or parallel to the maximum shear stress range for all fatigue tests in this study. This observation helps explain the improved representation of fatigue damage with either von Mises effective stress or the Findley approach. Since microscopic data for the fatigue crack initiation orientations were not available, only macroscopic two-dimensional observations will be discussed. Representative physical observations of the cracking behavior for similar combined in-phase and out-of-phase loadings are shown in Figs. 17 and 18, respectively. Maximum local shear stress amplitude orientations on the notch surface plane are shown with two parallel arrows, while the maximum local principal stress orientation(s) are shown with an arrow perpendicular to the maximum local shear stress amplitude plane.

Multiple crack initiation occurred at the weld toe for the in-phase combined bending-torsion tests. The actual cracking directions in the vicinity of the initiation site (points "I" in Fig. 17) agreed reasonably well with those predicted by the Findley model. As these cracks grew longer, the cracking direction changed perpendicular to the maximum local principal stress range. Visual observations indicated that crack growth in the maximum local principal stress orientation occurred for no more than the last 20% of the total fatigue life. At the onset of final fracture, the growth direction again followed the orientation of the maximum local shear stress range (point "F" in Fig. 17). This is probably a ductile failure mode of the base material and and is an insignificant fatigue life fraction. For these tests, crack initiation and growth in the maximum shear stress direction

dominated the fatigue life fraction (more than 80%). The behavior shown was typical for all in-phase tests.

For comparison, a similar out-of-phase test with $\lambda = 2.39$ was considered. Again, multiple crack initiation took place on the maximum local shear stress amplitude orientation (points "I" in Fig. 18). Due to the stress history characteristics of the out-of-phase loading, the maximum local principal and shear stress amplitudes are no longer 45° apart. For the out-of-phase loading case considered, both the dominant local principal and shear stress amplitudes are within ±13° of the notch root. The differentiation between local shear and principal stress controlled crack growth is more difficult than for the in-phase tests. Again, macroscopic crack growth comprised less than the final 20% of the fatigue life. However, if the local principal stress models were appropriate, the surface cracking characteristics would be similar to the in-phase test, since identical magnitude and orientation of fatigue damage is predicted for both loading cases. The macroscopic crack growth reflects the maximum shear stress range orientation predicted by the Findley model. At the onset of final failure, cracking occurred again on the maximum local shear stress orientation.

4.3 EFFECTS OF λ - RATIO

It is important to note that only one bending - to - shear stress ratio ($\lambda = 2.39$) was employed in this investigation to compare in-phase and out-of-phase fatigue tests. However, this value of λ falls within a range experienced in typical bridge beam applications as was shown previously (Appendix A).

An increase in (λ) would cause the stresses to be more nearly bending and, hence, the differences in fatigue damage between in-phase and out-of-phase loading cases would probably be less significant. On the other hand, the location of the weld on a web would also be important, since (λ) increases towards the neutral axis. Overall, it is believed that further studies with different λ - ratios are required to clarify the significance of out-of-phase loading to welded connections.

4.4 IMPLICATIONS FOR FATIGUE DESIGN PRACTICE

Although the (remote) principal stress-based design criteria are accepted by researchers for the fatigue design of weldments, most laboratory fatigue tests which are the basis of current structural design codes have been conducted using in-phase loading (uniaxial or three/four point bending). However, real structures often support moving loads which induce rotating principal stresses, since the stress components are not in

phase. The principal-stress-based approaches predict equal fatigue damage for any in-phase or out-of-phase loading for a given amplitude of maximum principal stress. In other words, the loading path dependency of fatigue damage is not reflected by the current principal-stress-based design criteria.

A typical example of (remote) principal-stress-based fatigue design codes for structural weldments is the British Standard BS 5400 [1]. In BS 5400, it is recommended that the mean minus two standard deviations curve will be used for general design purposes. The proper category for beams with web stiffener welds is the Class E. However, when comparing the Class E mean S_1-N_f curve for a stress level corresponding to $2 \cdot 10^6$ cycles to that of mean minus two standard deviations S_1-N_f curve, the difference in life for the same principal stress range differs by a factor of 3.33. However, in this investigation, the experimental difference in fatigue life between in-phase and out-of-phase stress histories producing identical principal stress ranges was a factor of 10. This observation indicates that even the BS 5400 mean minus two standard deviations design S_1-N_f curve for Class E joints is non-conservative. It would therefore appear that principal stress-based design approaches may severely underestimate the fatigue damage for out-of-phase, nonproportional biaxial loading cases even with the generous cushion of two standard deviations from the constant amplitude test data mean.

Similar comments apply to the "hot-spot" strain method used to evaluate the fatigue strength of welded offshore tubular joints subjected to in-phase laboratory fatigue loading [83, 84]. The "hot-spot" approach involves the measurement of (remote) axial strain, and no attempt is made to distinguish between in-phase and out-of-phase loading. Only (remote) strains perpendicular to the weld toe are measured; hence, the shear strain history is not captured. The method does not consider the local, notch-root stresses or strains.

The current ASME Boiler and Pressure vessel Code [85] employs Tresca's criteria for out-of-phase-loading situations. The maximum shear stress range during a loading cycle is to be found in a way similar to that discussed in Chapter 3.2. The Tresca criterion, while being a shear-based model, predicts both magnitude and orientation of fatigue damage; hence, the path dependency of fatigue damage is accounted for. However, the normal stresses on the maximum shear stress amplitude orientation are not considered in this analysis method. Since there are generally normal stresses on all orientations during out-of-phase loading, it is not surprising that non-conservative fatigue life estimates result for loading situations where the stress components are out-of-phase.

Findley's model based either on remote or local stresses shows promise in more accurately modelling the actual fatigue damage mechanisms and hence accounts for path dependent fatigue damage. Recent studies on thick-walled pressure vessels [86] have shown that even when the applied loading is in in-phase, Findley's model leads to more accurate fatigue life estimates than those based on principal stresses. Since shear and normal stresses dictate fatigue damage for the materials and specimen geometry employed in this investigation, critical plane approaches, such as Findley's model, appears to be a more accurate method of evaluating fatigue damage and are valid for both in-phase and out-of-phase loading.

The experimental differences in fatigue life between moving and stationary loading cases is probably not as reflected in actual bridge behavior due to the conservativeness of the current approaches. In the fatigue design of bridge members, the maximum design stresses, corrections to these for the lateral distribution of the vehicular loads, and corrections to these for the effects of impact are calculated based on extreme loading conditions that seldom occur [87] at all and certainly not simultaneously. However, these conservative assumptions do not change the fact that bridge beams experience out-of-phase, nonproportional stress-time histories, which the current principal stress-based design practice are unable to recognize. Shear stress-based models, such as Findley's critical plane approach, might serve as an alternate design approach in the future to reduce the conservativeness in the design practice by accounting for the loading path dependency of fatigue damage.

5. CONCLUSIONS

1. The fatigue life of the tube-to-plate weldments was found to be load path-dependent for a bending to shear stress ratio $\lambda = 2.39$. For the load history considered, in-phase loading was found to give an order of magnitude longer fatigue life than an out of phase loading having the same principal stresses.

2. Approximately 80% of the total fatigue life of the tube-to-plate weldments was spent in initiating multiple fatigue cracks in the life regime of 10^5 to 10^7 cycles for all loading paths studied. The initial cracks formed at the weld toe and were oriented parallel to the maximum local shear stress.

3. The tests results for both the in-phase and out-of-phase load histories could be correlated using Findley's equivalent shear stress model. The in-phase and out-of-phase test data could not be correlated using a maximum principal stress model, but a model based on the von Mises effective stress did better than the former but not as well as Findley's model.

4. Findley's model was most sensitive to mean stresses possibly because the mean normal stressed relaxed early in fatigue life leaving only the normal stress amplitude and the maximum shear stress amplitude to control the fatigue damage.

5. Current structural fatigue design codes for bridge beams employ the maximum amplitude of principal stress as a design parameter. Possible differences in fatigue life between moving (out-of -phase) and stationary (in-phase) loading cases are not reflected by these current methods of analysis.

6. LIST OF REFERENCES

1. BS5400: Part 10, 1980: "Steel, Concrete and Composite Bridges Part 10: Code of Practice for Fatigue", British Standards Institution, 1980.

2. Gurney, T. R.: "Fatigue Design Rules for Welded Steel Joints", The Welding Institute Research Bulletin, Vol. 17, May 1976, pp. 115-124.

3. Eide, O. I.: "On Cumulative Fatigue Damage in Steel Welded Joints", Report UR-83-30, Department of Marine Technology, The Norwegian Institute of Technology, The University of Trondheim, Norway, 1983, p. 102.

4. Berge, S. and Eide, O. I.: "Residual Stress and Stress Interaction in Fatigue Testing of Welded Joints", Residual Stress Effects in Fatigue, ASTM STP 776, American Society for Testing and Materials, 1982, pp. 115-131.

5. Maddox, S. J.: "Influence of Tensile Residual Stresses on the Fatigue Behavior of Welded Joints in Steel", Residual Stress Effects in Fatigue, ASTM STP 776, American Society for Testing and Materials, 1982, pp. 63-96.

6. "AASHTO Standard Specifications for Highway Bridges", Thirteenth Edition, The American Association of State Highway and Transportation Officials, 1983, Article 10.3, pp. 109-113.

7. "Byggsvetsnorm StBk-N2", Statens Stålbyggnadskommitte, Svetskommissionen, AB Svensk Byggtjänst, Stockholm, Sweden, 1974.

8. "Welding: Load Capacity of Welded Joints in Fatigue Loaded Steel Structures", SFS 2378, Finnish Standards Committee, Helsinki, Finland, 1985.

9. Reemsnyder, H. S.: "Development and Application of Fatigue Data for Structural Steel Weldments", Fatigue Testing of Weldments, ASTM STP 648, D. W. Hoeppner, Ed., American Society for Testing and Materials, 1978, pp. 3-21.

10. Fisher, J. W., Frank, K. H., Hirt, M. A. and McNamee, B. M.: "Effect of Weldments on the Fatigue Strength of Steel Beams", National Cooperative Highway Research Program (NCHRP) Report 102, Highway Research Board, National Research Council, Washington, D.C., 1970, 114 p.

11. Fisher, J. W., Albrecht, P. A., Yen, B. T., Klingerman, D. J.and McNamee, B. M.: "Fatigue Strength of Steel Beams with Welded Stiffeners and Attachments", National Cooperative Highway Research Program (NCHRP) Report 147, Transportation Research Board, National Research Council, Washington, D.C., 1974, 85 p.

12. Schilling, C. G., Klippstein, K. H., Barsom, J. M. and Blake G. T.: "Fatigue of Welded Steel Bridge Members Under Variable Amplitude Loadings", National Cooperative Highway Research Program (NCHRP) Report 188, Transportation Research Board, National Research Council, Washington, D.C., 1978, 113 p.

13. Gough, H. J., Pollard, H. V. and Clenshaw, W. J.: "Some Experiments on the Resistance of Metals to Fatigue Under Combined Stresses", Ministry of Supply, Aeronautical Research Council Reports and Memoranda No. 2522 (Monograph), His Majesty's Stationery Office, London, 1951, 141 p.

14. Thurston, R. C. A. and Field, J. E.: "The Fatigue Strength under Bending, Torsional and Combined Stresses of Steel Test Pieces with Stress Concentrations", Proceedings, The Institution of Mechanical Engineers, Vol. 164, 1954, pp. 785-792.

15. Findley, W. N.: "Fatigue of Metals Under Combinations of Stresses", Transactions of the ASME, The American Society of Mechanical Engineers, Vol. 79, 1956, pp. 1337-1348.

16. Findley, W. N. and Mathur, P. N.: "Modified Theories of Fatigue Failure Under Combined Stress", Proceedings of the Society for Experimental Stress Analysis, C.V. Mahlmann and W.M. Murray, Eds., Vol. 14, No. 1, Cambridge, Mass., 1956, pp.35-46.

17. Findley, W. N.: "Effect of Range of Stress on Fatigue of 76S-T61 Aluminum Alloy Under Combined Stresses Which Produce Yielding", Journal of Applied Mechanics, Paper No. 53-APM-12, The American Society of Mechanical Engineers, 1953, pp. 1-10.

18. Sines,G.: "Behavior of Metals Under Complex Static and Alternating Stresses", Metal Fatigue, G. Sines and J.L. Waisman, Eds., McGraw-Hill, New York, 1959, pp. 145-169.

19. Sines, G. and Ohgi, G.: "Fatigue Criteria Under Combined Stresses or Strains", Transactions of the ASME, Journal of Engineering Materials and Technology, Vol. 103, April 1981, pp. 82-90.

20. Lee, S. -B.: "A Criterion for Fully Reversed Out-of-Phase Torsion and Bending", Multiaxial Fatigue, ASTM STP 853, K. J. Miller and M. W. Brown, Eds., American Society for Testing and Materials, Philadelphia, 1985, pp. 553-568.

21. Tipton, S. M. and Nelson, D. V.: "Fatigue Life Predictions for a Notched Shaft in Combined Bending and Torsion", Multiaxial Fatigue, ASTM STP 853, K. J. Miller and M. W. Brown, Eds., American Society for Testing and Materials, Philadelphia, 1985, pp. 514-550.

22. Tipton, S. M.: "Multiaxial Fatigue Life Predictions for the SAE Specimen Using Stress Based Approaches", Multiaxial Fatigue - Analysis and Experiments, G. E. Leese and D. F. Socie, Eds., Society of Automotive Engineers, Inc., Warrendale, PA, 1989, Chapter 4, pp. 61-65.

23. ASME Boiler and Pressure Vessel Code, Section III, Division I, Subsection NA, Appendix XIV, American Society of Mechanical Engineers, New York, NY 1978.

24. "Cases of the ASME Boiler and Pressure Vessel Code", Code Case N-47-12, American Society of Mechanical Engineers, New York, NY 1978.

25. Stulen, F. B. and Cummings, H. N.: "A Failure Criterion for Multi-Axial Fatigue Stresses", Proceedings of the ASTM, Vol. 54, The American Society for Testing and Materials, 1954, pp. 822-835.

26. Guest, J. J.: "Recent Research on Combined Stress", Proceedings of the Institution of Automobile Engineers, Vol. 35, December 1940, pp. 33-72 and pp. 146-170.

27. Guest, J. J.: "The Problem of Combined Stress", Engineering - An Illustrated Weekly Journal, C. Cooper and J. F. Petree, Eds., Vol. 155, January to June 1943, pp. 21-23, 101-102, 222, 281-282, 303-304.

28. "Fatigue Performance Under Multiaxial Loading in Marine Structures", Draft Final Report, CRC Project No. 181-01, United States Coast Guard Contract No. DTCG23-88-C-20021, Columbia Research Corporation, 703 Giddings Avenue, Suite U-3, Annapolis, Maryland 21401, 1989, pp. 3.4-3.5.

29. Findley, W. N.: "Experiments in Fatigue Under Ranges of Stress in Torsion and Axial Load from Tension to Extreme Compression", Proceedings of the ASTM, Vol. 54, The American Society for Testing and Materials, 1954, pp. 836-853.

30. Findley, W. N., Coleman, J. J. and Hanley, B. C.: "Theory for Combined Bending and Torsion Fatigue with Data for SAE 4340 Steel", Proceedings of the International Conference on Fatigue of Metals, London (10-14 September 1956), New York (28-30 November 1956), The Institution of Mechanical Engineers, 1956, pp. 150-157.

31. Findley, W. N.: "A Theory for the Effect of Mean Stress on Fatigue of Metals Under Combined Torsion and Axial Load or Bending", Journal of Engineering for Industry, November 1959, The American Society of Mechanical Engineers, pp. 301-306.

32. McDiarmid, D. L.: "Failure Criteria and Cumulative Damage in Fatigue Under Multi-Axial Stress Conditions", Ph.D. Thesis, Department of Mechanical Engineering, The City University, London, June 1972, 318 p.

33. Grubisic, V. and Simbürger, A.: "Fatigue Under Combined Out-of-Phase Multiaxial Stresses" International Conference on Fatigue Testing and Design, Society of Environmental Engineers, London, 1976, pp. 27.1-27.8.

34. Fash, J. W., Socie, D. F. and McDowell, D. L.: "Fatigue Life Estimates for a Simple Notched Component Under Biaxial Loading", Multiaxial Fatigue, ASTM STP 853, K. J. Miller and M. W. Brown, Eds., American Society for Testing and Materials, Philadelphia, 1985, pp. 497-513.

35. Senior, A. G. and Gurney, T. R.: "The Design and Service Life of the Upper Part of Welded Crane Girders", The Structural Engineer, Vol. 41, No. 10, October 1963, pp. 301-312.

36. Sedlmayer, F.: "Beanspruchung der Kranträgerobergurte durch die Radlasten der Laufkatze", Tech. Mitt. Krupp, Werksberichte, Band 29, H 3/4, Fried. Krupp GmbH Krupp Industrie- und Stahlbau Kranbau Wilhelmshaven, Berlin 1971, pp. 85-90.

37. Maas, G.: "Investigations Concerning Craneway Girders", Iron and Steel Engineer, Vol. 47, No. 3, March 1972, pp. 49-58.

38. Reemsnyder, H. S. and Demo, D. A.: "Fatigue Cracking in Welded Crane Runway Girders: Causes and Repair Procedures", Iron and Steel Engineer, Vol. 55, No. 4, April 1978, pp. 52-56.

39. Weiss, M. P.: "Simulation and Monitoring of Loads in Crane Beams", Service Fatigue Loads Monitoring, Simulation, and Analysis, ASTM STP 671, P.R. Abelkis and J.M. Potter, Eds., American Society for Testing and Materials, 1979, pp. 208-221.

40. Ingraffea, A. R., Gerstle, W. H., Mettam, K. I., Wawrzynek, P. and Heller, A. K.: "Cracking of Welded Crane Runway Girders: Physical Testing and Computer Simulation", Iron and Steel Engineer, Vol.62, No. 12, December 1985, pp. 46-52.

41. Patrikeev, A. B.: "Welding of Stiffening Ribs to Tensioned Flanges of Crane Beams", Svar. Proizvod., No. 3, 1975, pp. 26-28.

42. O'Connor, C. and Hung Tin Chan, T.: Dynamic Wheel Loads from Bridge Strains", ASCE Journal of Structural Engineering, Vol. 114, No. 8, August 1988, pp. 1703-1723.

43. O'Connor, C. and Hung Tin Chan, T.: "Wheel Loads from Bridge Strains: Laboratory Studies", ASCE Journal of Structural Engineering, Vol. 114, No. 8, August 1988, pp. 1724-1740.

44. Baldwin, T.: "Significance of the Fatigue of Metals to Railways", Proceedings of the International Conference on Fatigue of Metals, London (10-14 September),

New York (28-30 November), The Institution of Mechanical Engineers, London, UK, 1956, pp. 695-703.

45. Glinka, G. (University of Waterloo, Ontario, Canada) - Private communication.

46. Stallmeyer, J. E., Munse, W. H. and Lawrence, F. V., Jr. (University of Illinois at Urbana-Champaign, Illinois, USA) - Private communication.

47. Niemi, E. J. (Lappeenranta University of Technology, Finland) - Private communication.

48. Leese, G. E.: "Engineering Significance of Recent Multiaxial Research", Low Cycle Fatigue, ASTM STP 942, H.D. Solomon, G.R. Halford, L.R. Kaisand and B.N. Leis, Eds., American Society for Testing and Materials, Philadelphia, 1988, pp. 861-873.

49. Krempl, E.: "The Influence of State of Stress on Low-Cycle Fatigue of Structural Materials: A Literature Survey and Interpretive Report", ASTM STP 549, American Society for Testing and Materials, Philadelphia, 1974, 46 p.

50. Garud, Y. S.: "Multiaxial Fatigue: A Survey of the State of the Art", Journal of Testing and Materials, JTEVA, Vol. 9, No. 3, May 1981, pp. 165-178.

51. Brown, M. W. and Miller, K. J.: "Two Decades of Progress in the Assessment of Multiaxial Low-Cycle Fatigue Life", Low Cycle Fatigue and Life Prediction, ASTM STP 770, C. Amzallag, B. N. Leis and P. Rabbe, Eds., American Society for Testing and Materials, Philadelphia, 1982, pp. 482-499.

52. Ellyin, F. and Valaire, B.: "Development of Fatigue Failure Theories for Multiaxial High Strain Conditions", SM Archives, Vol. 10, 1985, Martinus Nijhoff Publishers, Dordrecht, pp. 45-85.

53. Kouba, N. G. and Stallmeyer, J. E.: "The Behavior of Stiffened Beams Under Repeated Loads", Structural Research Series No. 173 (unpublished), Civil Engineering Studies, University of Illinois at Urbana-Champaign, Urbana, Illinois, April 1959, 65 p.

54. Munse, W. H. and Stallmeyer, J. E.: "Fatigue in Welded Beams and Girders", Bridge Dynamics and Deflections and Fatigue in Welded Beams, Highway

Research Board Bulletin 315, National Academy of Sciences, National Research Council, Publication 961, Washington, D.C., 1962, pp. 45-62.

55. Moyar, G. J. and Garg, V. K.: "Biaxial Fatigue Design Procedure Applied to Welded Plate Structures" (unpublished), 21 p., private communication, Prof. W.H. Munse, University of Illinois at Urbana-Champaign.

56. Gurney, T. R. and Woodley, C. C.: "Investigation into the Fatigue Strength of Welded Beams. Part III: High Tensile Steel Beams with Stiffeners Welded to the Web", British Welding Journal, September 1962, pp. 533-539.

57. Barsom, J. M. and Rolfe, S. T.: "Fracture & Fatigue Control in Structures: Applications of Fracture Mechanics", Second Edition,Prentice Hall, Inc., Englewood Cliffs, NJ, 1987, pp. 438-442.

58. Yung, J.-Y. and Lawrence, F. V., Jr.: "Predicting the Fatigue Life of Welds Under Combined Bending and Torsion", Report No. 125, College of Engineering, University of Illinois at Urbana-Champaign, Urbana, Illinois, 1986, 27 p.

59. Archer, R.: "Fatigue of Welded Steel Attachments under Combined Direct Stress and Shear Stress", Paper No. 50, International Conference on Fatigue of Welded Constructions, The Welding Institute, 7-9 April, Brighton, UK, 1987, pp. P50.1-P50.10.

60. Story, K. and Mason, P.: "X-Ray Diffraction Determination of the Surface Principal Residual Stresses in Two Mild Steel Tube-to-Plate Welded Samples", Report No. 0051-0005, Lambda Research, Inc., Cincinnati, OH, 1989.

61. Tiitto, K. (American Stress Technologies, Inc., Pittsburgh, PA)- Private communication, 1989.

62. Downing, S. D. and Galliart, D. R.: "A Fatigue Test System for a Notched Shaft in Combined Bending and Torsion", Multiaxial Fatigue, ASTM STP 853, K. J. Miller and M. W. Brown, Eds., American Society for Testing and Materials, Philadelphia, PA, 1985, pp. 24-32.

63 Stallmeyer, J. E. and Lawrence, F. V., Jr. (University of Illinois at Urbana-Champaign, Illinois, USA) - Private Communication.

64 Walker, W. H. and Ruhl, J. A.: "Stress Histories for Highway Bridges Subjected to Traffic Loading", Final Report on the Investigation of Dynamic Stresses in Highway Bridges, Project IHR-85, Illinois Cooperative Higway Research Program, University of Illinois at Urbana-Champaign, Urbana, Illinois, April 1975.

65 Walker, W. H.: "Stress History Studies and the Fatigue Life Expectancy of Highway Bridges", Final Report on Life Life Expectancy of Highway Bridges - Stress History Studies, Project IHR-301, Illinois Cooperative Higway Research Program, University of Illinois at Urbana-Champaign, Urbana, Illinois, April 1980.

66. "Steel Construction", Manual of the American Institute of Steel Construction, Fifth Edition, American Institute of Steel Construction, New York, NY 1959, p. 12.

67. PATRAN Plus User Manual Vol 1 & 2, P/N-2191001, Release 2.3, PDA Engineering, Patran Division, 2975 Redhill Avenue, Costa Mesa, CA 92626, July 1988,

68. Jakubczak, H. and Glinka, G.: "Fatigue Analysis of Manufacturing Defects in Weldments", International Journal of Fatigue, Vol. 8, No. 2, 1986, pp. 51-57.

69. Bokarlund, T. and Karlsen, A.: "Control of Fatigue Failure in Ship Hulls by Ultrasonic Inspection", Norwegian Maritime Research, No. 1, 1982, pp. 9-15.

70. Engesvik, K. M. and Moan, T.: "Probabilistic Analysis of the Uncertainty in the Fatigue Capacity of Welded Joints", Engineering Fracture Mechanics, Vol. 18, No. 4, 1983, pp. 743-762.

71. Bell, R., Vosikovsky, O. and Bain, S. A.: "The Significance of Weld Toe Undercuts in the Fatigue of Steel Plate T-Joints", International Journal of Fatigue, Vol. 11, No. 1, 1989, pp. 3-11.

72. Smith, I. F. C. and Smith, R. A.: "Defects and Crack Shape Development in Fillet Welded Joints", Fatigue of Engineering Materials and Structures, Vol. 5, No. 2, 1982, pp. 151-165.

73. Otegui, J. L., Kerr, H. W., Burns, D. J. and Mohaupt, U. H.: "Fatigue Crack Initiation from Defects at Weld Toes in Steel", International Journal of Pressure Vessels & Piping, Vol. 38, 1989, pp. 385-417.

74. Lawrence, F. V., Jr., Mattos, R. J., Higashida, Y. and Burk, J. D.: "Estimating the Fatigue Crack Initiation Life of Welds", Fatigue Testing of Weldments, ASTM STP 648, D.W. Hoeppner, Ed., American Society for Testing and Materials, 1978, pp. 134-158.

75. ABAQUS User's Manual, version 4.7. Hibbitt, Karlsson and Sorensen, Inc., 1988.

76. Siljander, A., Kurath, P. and Lawrence, F.V. , Jr.: "Multiaxial Nonproportional Fatigue of Weldments", Proceedings of the 9th International Conference on Offshore Mechanics and Arctic Engineering, Vol. III, Part A, 1990, the American Society of Mechanical Engineers, pp. 229-237.

77. Morrow, J.: "Cyclic Plastic Strain Energy and Fatigue of Metals", Internal Friction, Damping, and Cyclic Plasticity, ASTM Special Technical Publication No. 378, The American Society for Testing and Materials, 1964, p. 45.

78. Basquin, O. H.: "The Exponential Law of Endurance Tests", Proceedings of the ASTM, Vol. 10, Part II, American Society for Testing and Materials, 1910, p. 625.

79. Youshi, H., Yonghua, L. and Zhemin, Z., "Initiation and propagation of short fatigue cracks in a weld metal," Fatigue Fractures in Engineering Materials and Structures, Vol. 12, No. 4, 1989, pp. 323-331.

80. Kurath, P. and Socie, D. F.: "The Relationship Between Observed Fatigue Damage and Life Estimation Models", NASA Contractor Report No. 182191, National Aeronautics and Space Administration, August, 1988, 42 p.

81. Peterson, R. E.: "Analytical Approach to Stress Concentration Effect in Fatigue of Aircraft Materials", Proceedings of the Symposium on Fatigue of Aircraft Structures, 1959 USAF-WADC Technical Report 59-707, Dayton, OH, August, 1959.

82. Kurath, P. and Fatemi, A.: "Multiaxial Fatigue Life Predictions under the Influence of Mean Stress", Transactions of the ASME, Journal of Engineering Materials and Technology, Vol. 110, No. 10, pp. 380-388, 1988.

83. Marshall, P. W.: "Fatigue Design Rules in the U. S. A.", Proceedings of the 9th International Conference on Offshore Mechanics and Arctic Engineering, Vol. III, Part A, 1990, the American Society of Mechanical Engineers, pp. 175-184.

84. API Recommended Practice for Planning, Designing and Constructing Fixed Offshore Platforms, API RP 2A, Fifteenth Edition, American Petroleum Institute, Washington, D. C., October 22, 1984, 115 p.

85. ASME Code Section III (Nuclear Power Plant Components), Article XIV-1000, Design Based on Fatigue Analysis, The American Society of Mechanical Engineers, New York, NY, 1986, pp. 405-407.

86. Burns, D. (University of Waterloo, Ontario, Canada) - Private communication.

87. Melhem, H. G. and Klippstein, K. H.: "A Study on Variable Amplitude Load Fatigue: Work In Progress", Research Report No. ST-6, Department of Civil Engineering, University of Pittsburgh, Pennsylvania, January 1990, pp. 12 - 16.

Table 1

MECHANICAL PROPERTIES OF ASTM A519 COLD-DRAWN STEEL TUBING AND ASTM A36 HOT-ROLLED STEEL PLATE.

Material	Property		
	σ_Y (MPa)	σ_U (MPa)	E (MPa)
ASTM A519	550	700	205,000
ASTM A36	224	414	205,000

Table 2

SUMMARY OF THE RESIDUAL STRESS MEASUREMENTS USING X-RAY DIFFRACTION [60].

Specimen condition	Orientation (degrees)			
	-45	0 (longitudinal)	45	90* (circumferential)
As-welded	-559 MPa	-497 MPa	-448 MPa	-510 MPa
Stress-relieved	+67 MPa	-9 MPa	+20 MPa	+96 MPa

Table 3

SUMMARY OF THE NOMINAL LOADING CONDITIONS FOR THE STRESS-RELIEVED TUBE-TO-PLATE WELDED SPECIMEN.

Load path	Specimen number	λ	R_σ	R_τ	S_x^{max} (MPa)	Γ_{xz}^{max} (MPa)	Fatigue life (cycles)
A	113	∞	-1	-	220.0	0.0	76,800
	108	∞	-1	-	158.5	0.0	276,400
	110	∞	-1	-	140.0	0.0	395,900
	111	∞	-1	-	110.0	0.0	729,900
B	112	∞	0	-	440.0	0.0	55,700
	4	∞	0	-	280.0	0.0	270,390
	107	∞	0	-	207.7	0.0	1,036,000
	5	∞	0	-	220.0	0.0	1,300,140
	1	∞	0	-	140.0	0.0	> 5,000,000
	114	∞	0	-	155.0	0.0	> 16,000,000
C	304	0	-	-1	0.0	110.0	132,000
	301	0	-	-1	0.0	110.0	141,460
	300	0	-	-1	0.0	85.0	1,605,000
	302	0	-	-1	0.0	70.0	3,303,000
	305	0	-	-1	0.0	70.0	1,988,970
	115	0	-	-1	0.0	72.6	> 15,600,000
D	7	0	-	0	0.0	220.0	374,000
	8	0	-	0	0.0	170.0	919,600
F	106	2.39	0	0	260.3	108.9	260,200
	105	2.39	0	0	260.3	108.9	274,700
	15	7.34	0	0	216.1	29.4	577,000
	14	7.34	0	0	216.1	29.4	748,600
	2	1.0	0	0	136.0	136.0	852,900
	12	2.39	0	0	174.0	72.6	1,196,100
	11	2.39	0	0	174.0	72.6	1,201,400
	13	2.39	0	0	174.0	72.6	1,699,800
	9	2.39	0	0	174.0	72.6	> 3,000,000
	3	1.0	0	0	80.3	80.3	> 10,000,000
G	109	2.39	+1	-1	174.0	72.6	6,020,400
H	101	1	+1	0	170.0	170.0	981,200
I	6	2.39	0	-1	174.0	72.6	111,500
	10	2.39	0	-1	174.0	72.6	142,600
	16	2.39	0	-1	174.0	72.6	167,900
	100	2.39	0	-1	174.0	72.6	206,300
	115A	2.39	0	-1	143.3	59.8	411,958
	116	2.39	0	-1	119.8	50.0	> 3,927,330
	117	2.39	0	-1	119.8	50.0	> 7,082,660
J	102	2.39	0	0	174.0	72.6	352,500
	103	2.39	0	0	174.0	72.6	354,200
	104	2.39	0	0	174.0	72.6	644,500

Table 4

SUMMARY OF FINITE ELEMENT STRESS AND STRAIN CONCENTRATION FACTORS (WELD TOE RADIUS R = 0.18 MM).

SCF	Bending only $\lambda = \infty$	Torsion only $\lambda = 0$	Combined $\lambda = 2.39$
K_{σ_1}	5.07	3.03	4.80
$K_{\sigma_{eff}}$	3.30	2.94	3.16
K_{ε_1}	3.89	3.07	3.79
$K_{\varepsilon_{eff}}$	4.40	3.04	3.74

Table 5

SUMMARY OF FINITE ELEMENT STRESS AND STRAIN CONCENTRATION FACTORS (WELD TOE RADIUS R = 4.0 MM).

SCF	Bending only $\lambda = \infty$	Torsion only $\lambda = 0$	Combined $\lambda = 2.39$
K_{σ_1}	1.52	1.29	1.50
$K_{\sigma_{eff}}$	1.34	1.33	1.33
K_{ε_1}	1.41	1.30	1.43
$K_{\varepsilon_{eff}}$	1.76	1.33	1.59

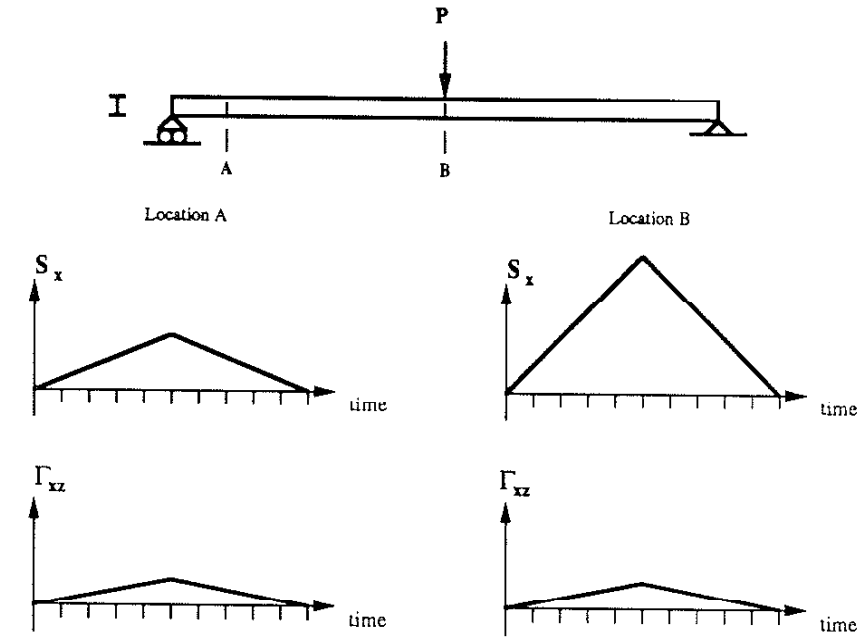

(a)

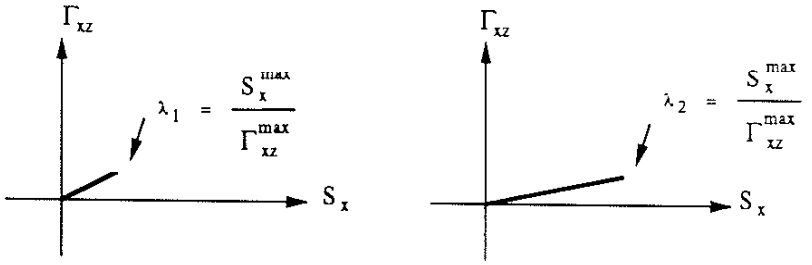

(b)

Figure 1 (a) Bending and shearing stress in-phase time histories in the vicinity of the span center and 0.1 x span length of the bridge beam with a stationary load. (b) An alternate representation of the in-phase bending-shear relations shown in Fig. 1a.

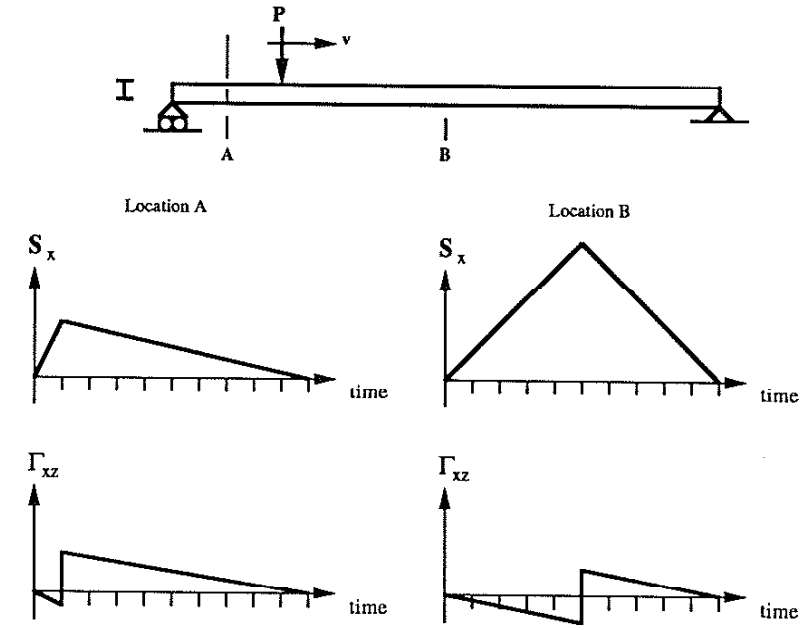

(a)

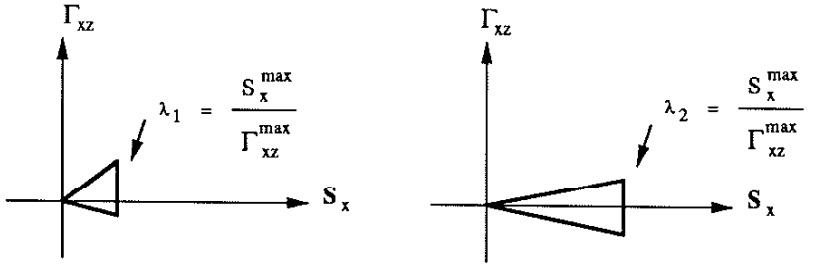

(b)

Figure 2 (a) Bending and shearing stress out-of-phase time histories in the vicinity of the span center and 0.1 x span length of the bridge beam with a moving load.
(b) An alternate representation of the out-of-phase bending-shear relations shown in Fig. 2a.

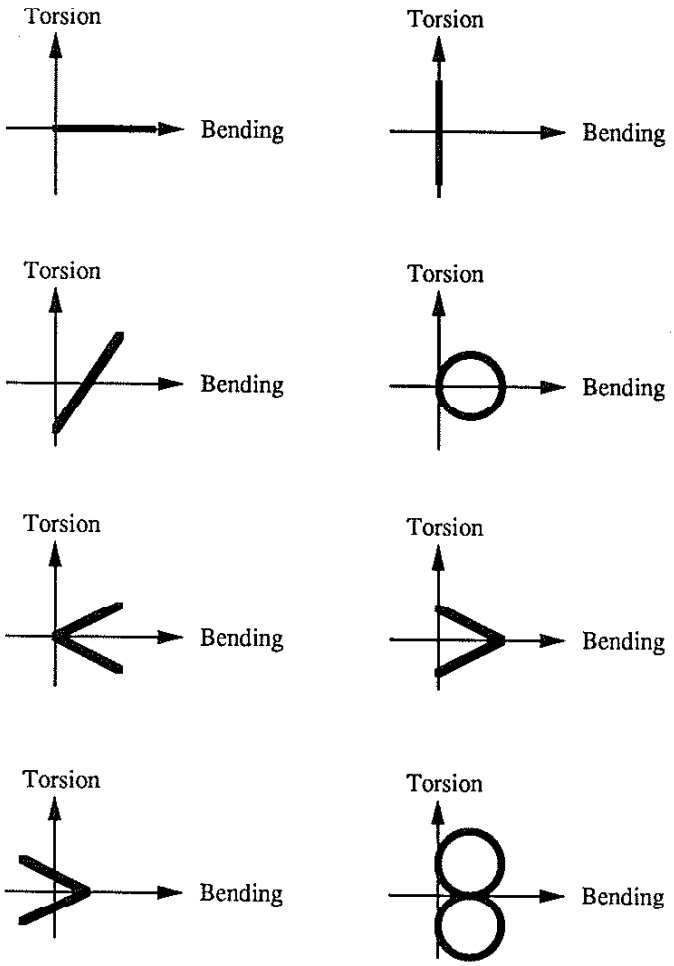

Figure 3 Summary of the biaxial in-phase and out-of-phase loading paths employed by Archer [59].

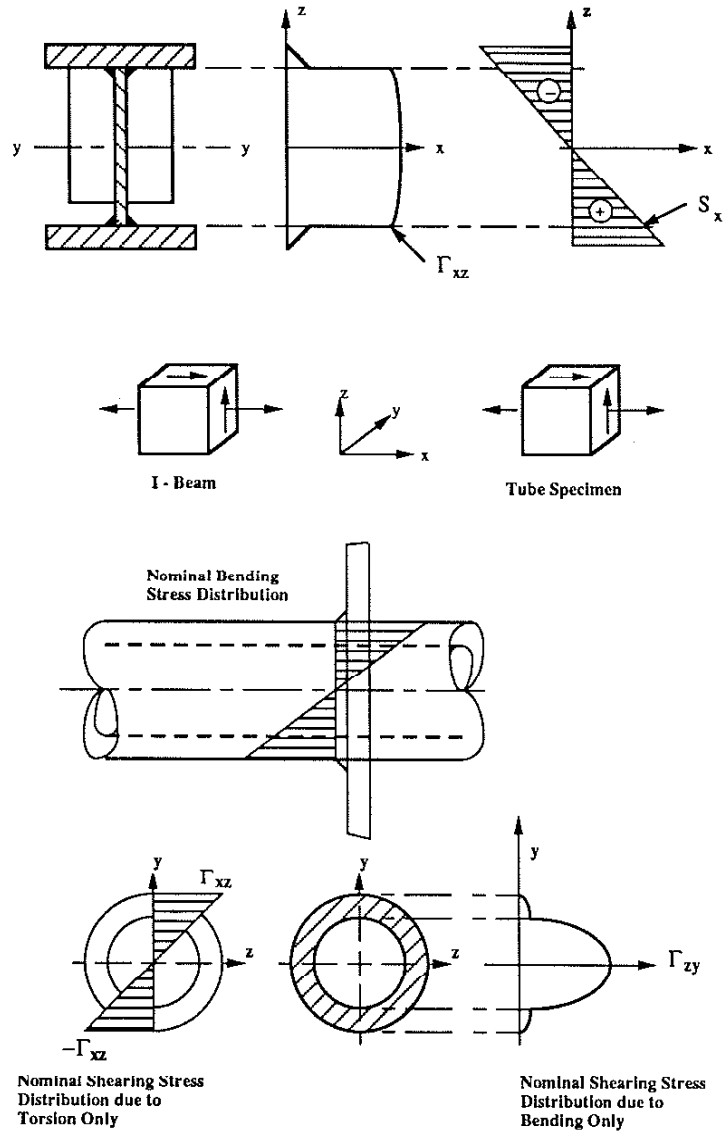

Figure 4 Similitude assumption of nominal stresses between a large-scale structure and the tube-to-plate welded specimen.

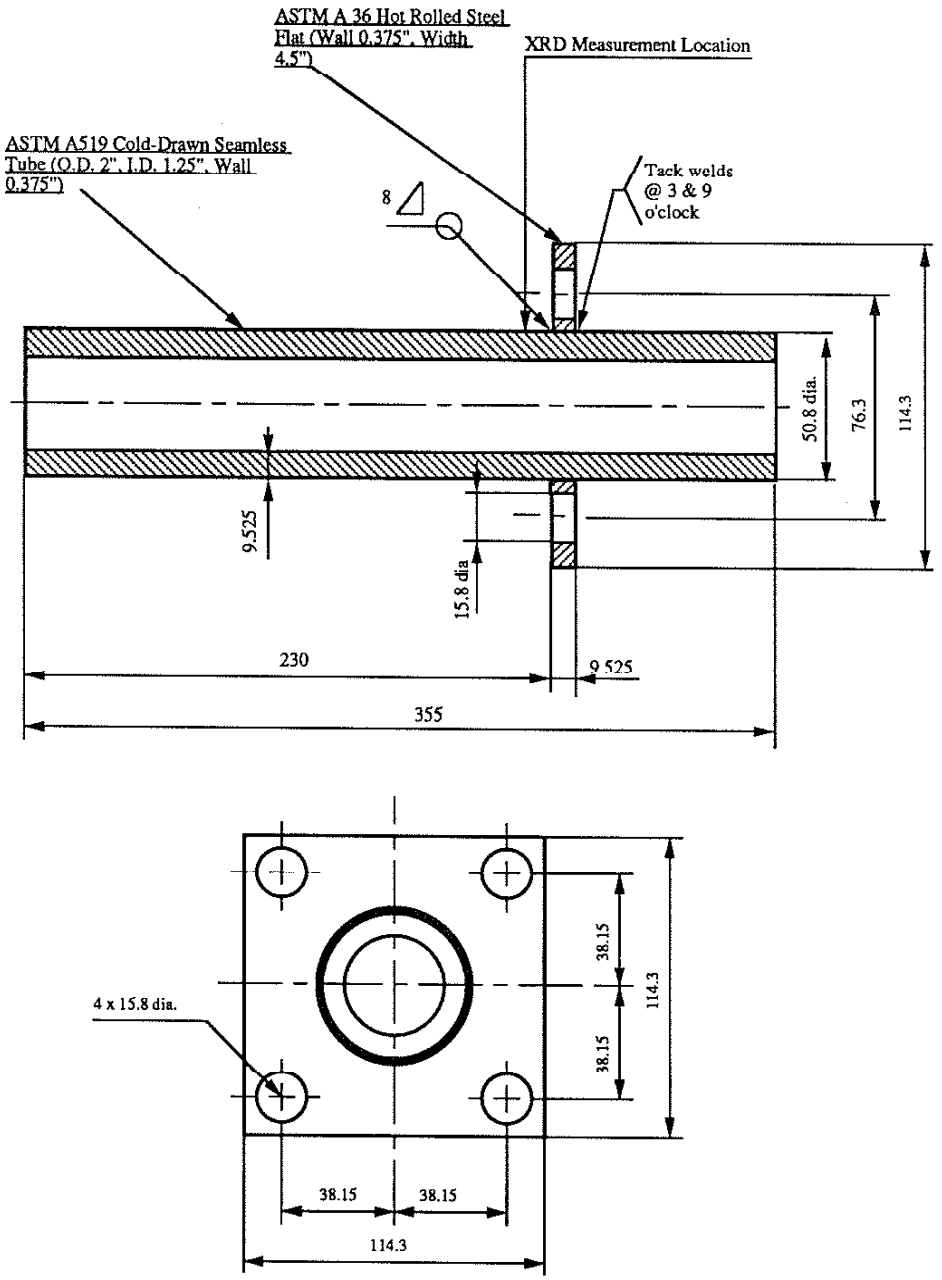

Figure 5 The dimensions of the tube-to-plate welded specimen.

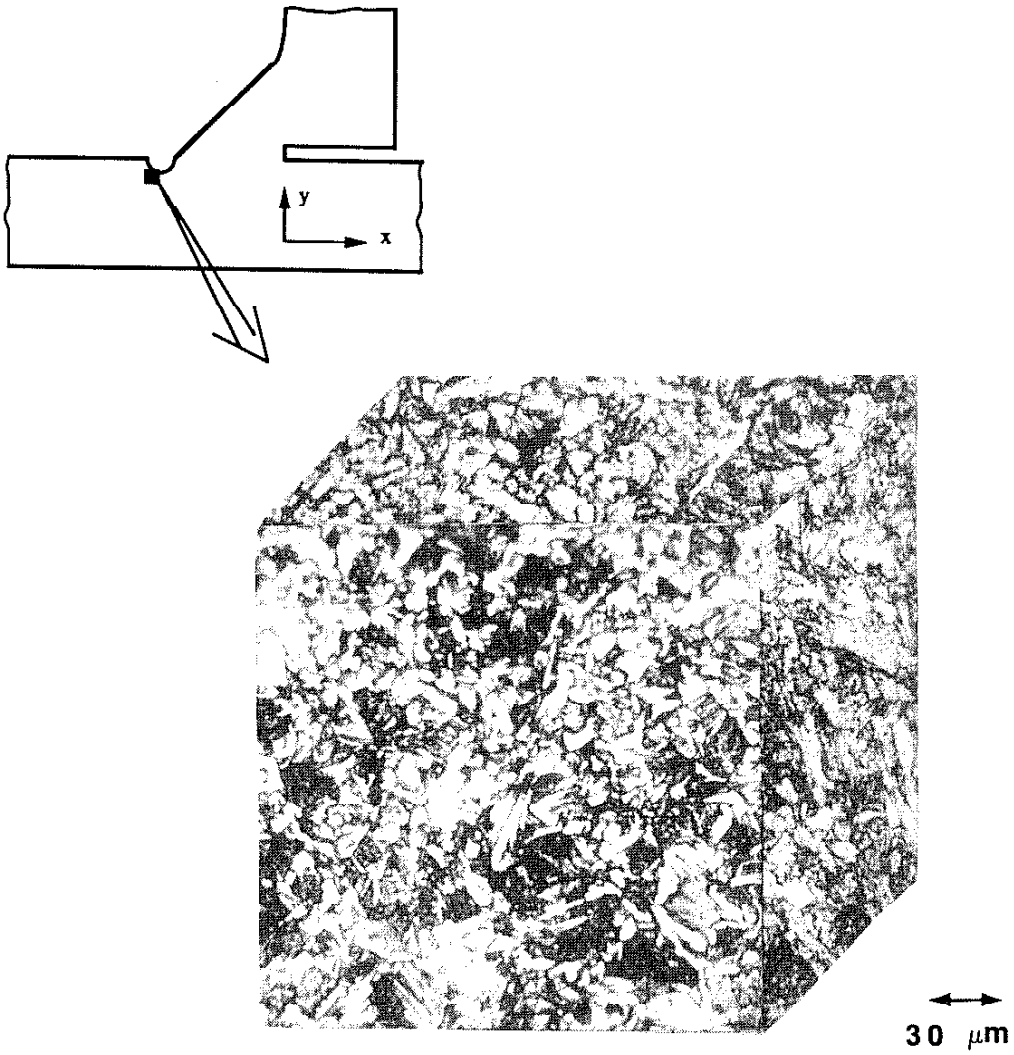

Figure 6 Microstructure of the material in the vicinity of the fatigue crack initiation site in the heat-affected-zone, 320 X (2% Nital etch).

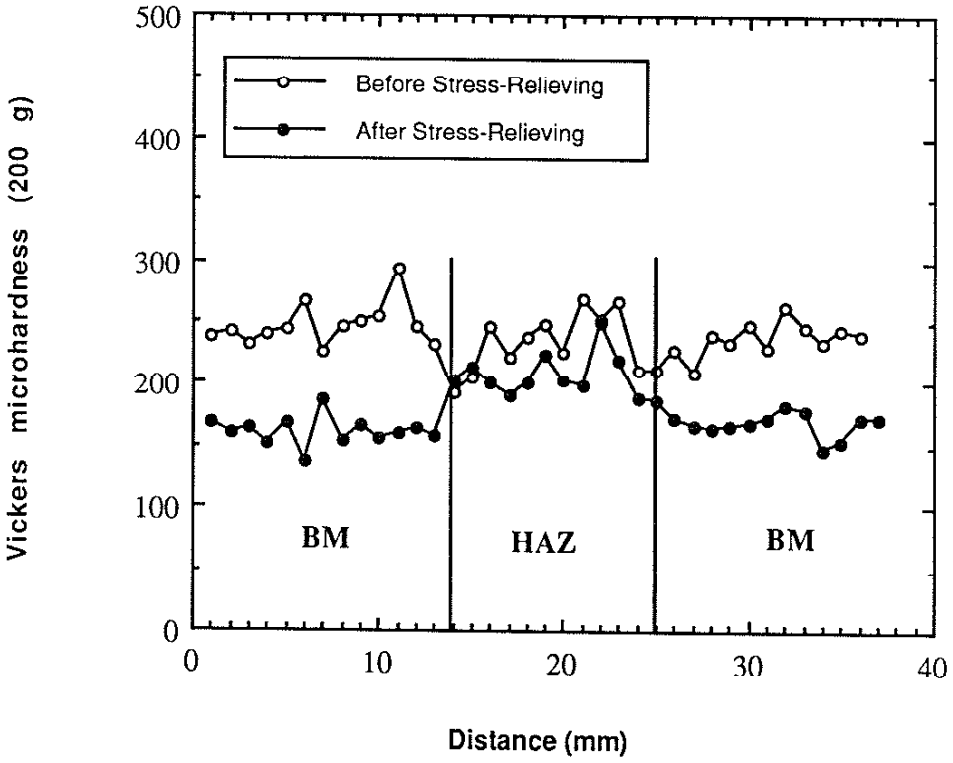

Figure 7 Vickers microhardness profile of the tube-to-plate welded joint (measured at 1 mm below and parallel to the surface of the tube).

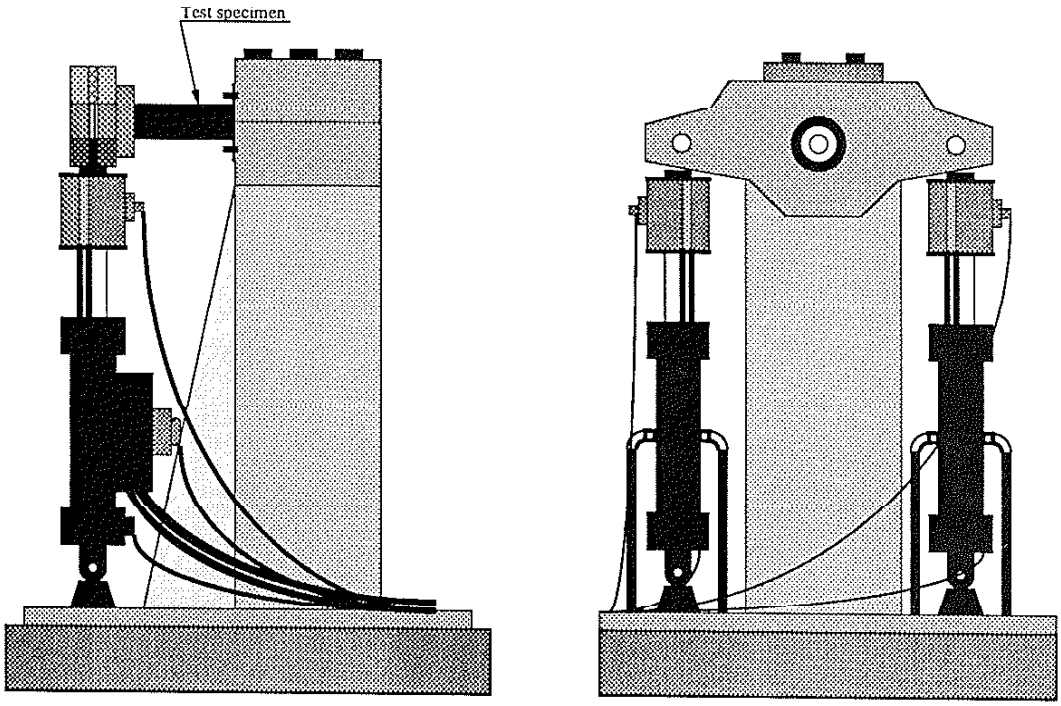

Figure 8 Schematic side and front view of the SAE fatigue test facility employed to test the tube-to-plate welded specimen.

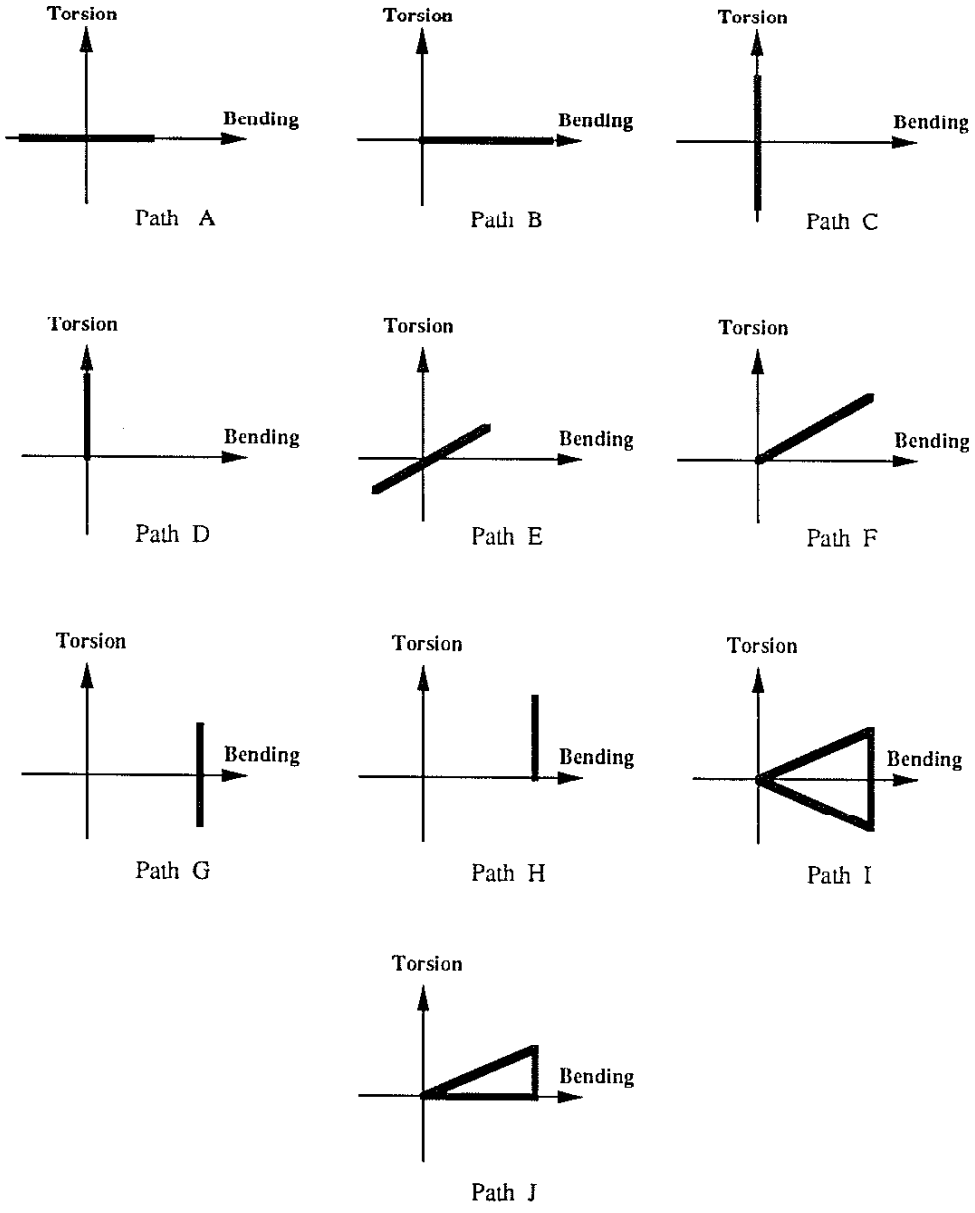

Figure 9 Summary of the loading paths employed in the in-phase and out-of-phase biaxial fatigue tests.

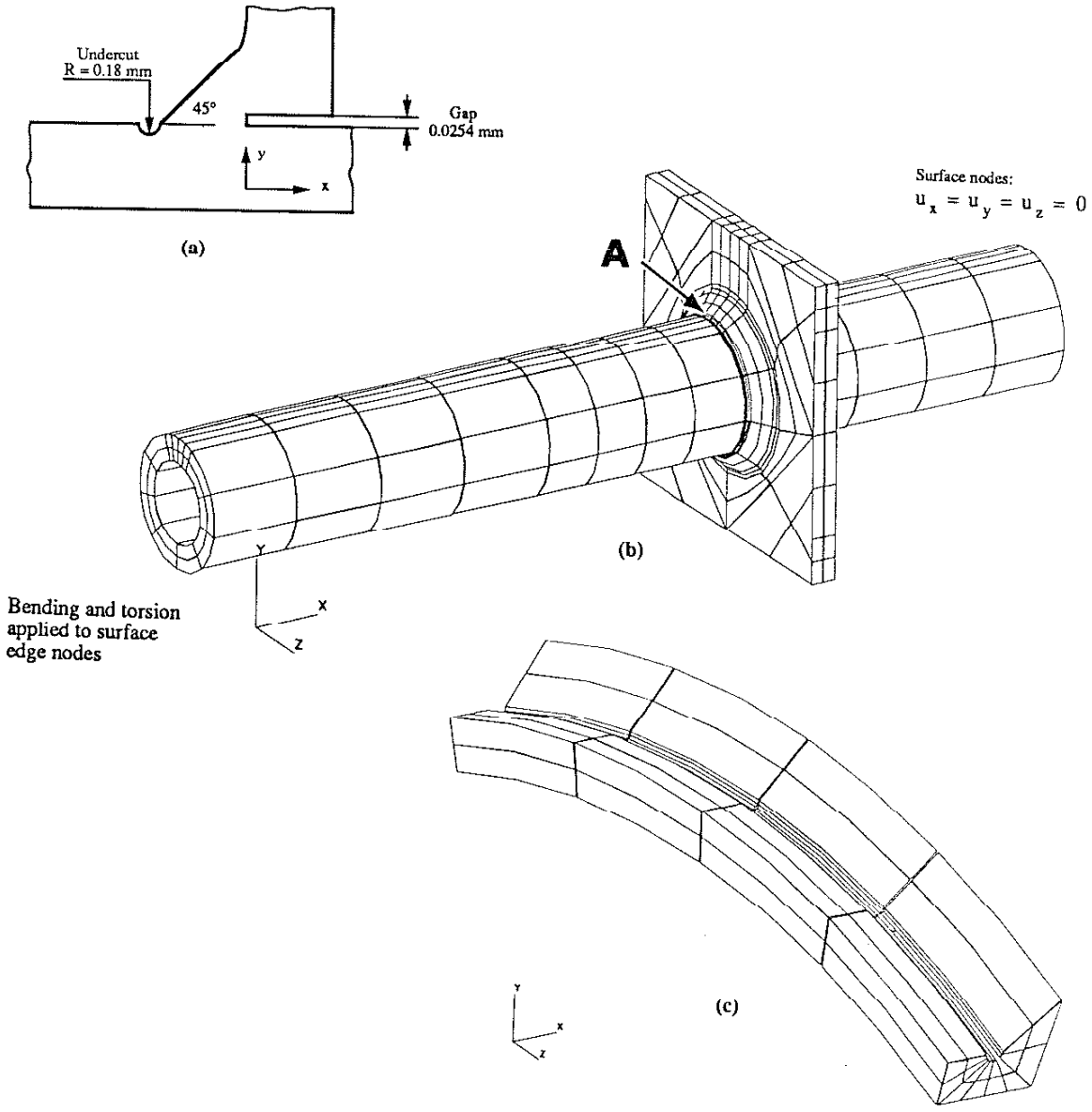

Figure 10 Schematic side view of the undercut in the global xy-plane (a), three-dimensional view of the finite element model of the tube-to-plate welded specimen (b) and three-dimensional close-up view of the undercut (c).

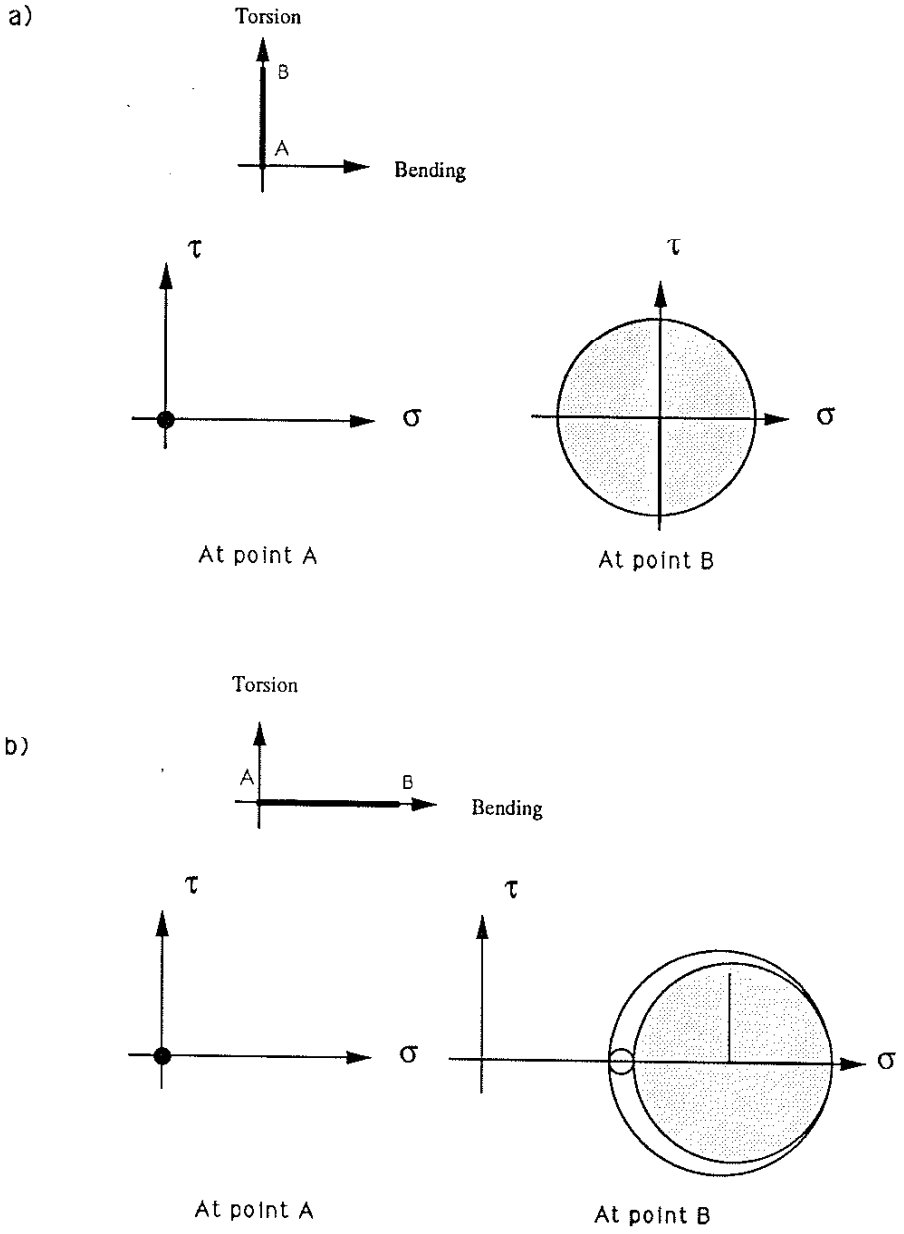

Figure 11 Generalized nominal loading path and local Mohr's stress circles at the critical location below surface for (a) torsional only and (b) bending only loading. Shaded circles represent the surface plane of the notch in three-dimensional stress space.

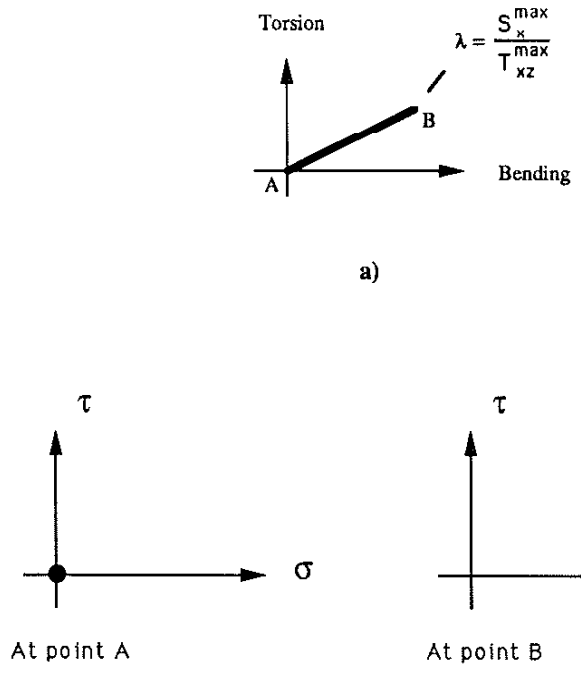

Figure 12 Generalized nominal loading path (a) and local Mohr's stress circles at the critical location below surface for in-phase combined bending-torsion (b). Shaded circles represent the surface plane of the notch in three-dimensional stress space.

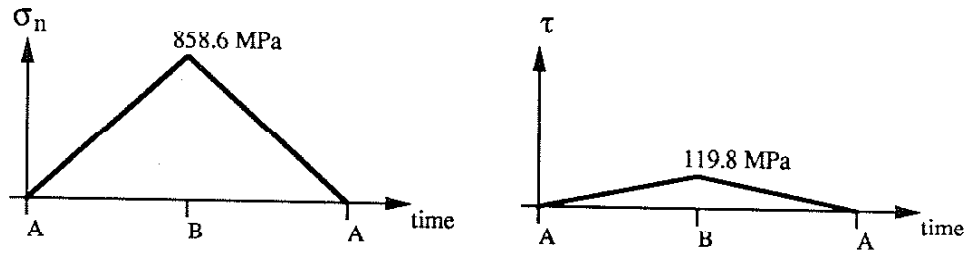

(c)

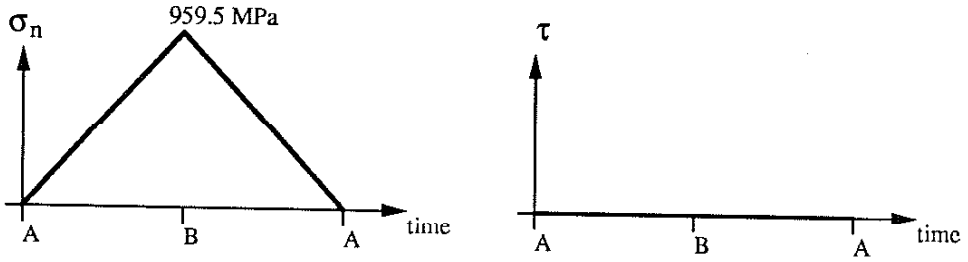

(d)

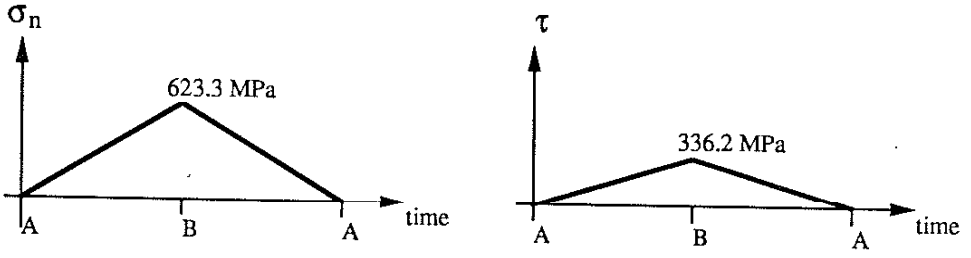

(e)

Figure 12 (Continued) Resulting normal and shearing stress-time histories in (c) longitudinal, (d) maximum local principal stress and (e) maximum local shear stress directions corresponding to the in-phase bending-torsion loading path shown in Fig. 12a.

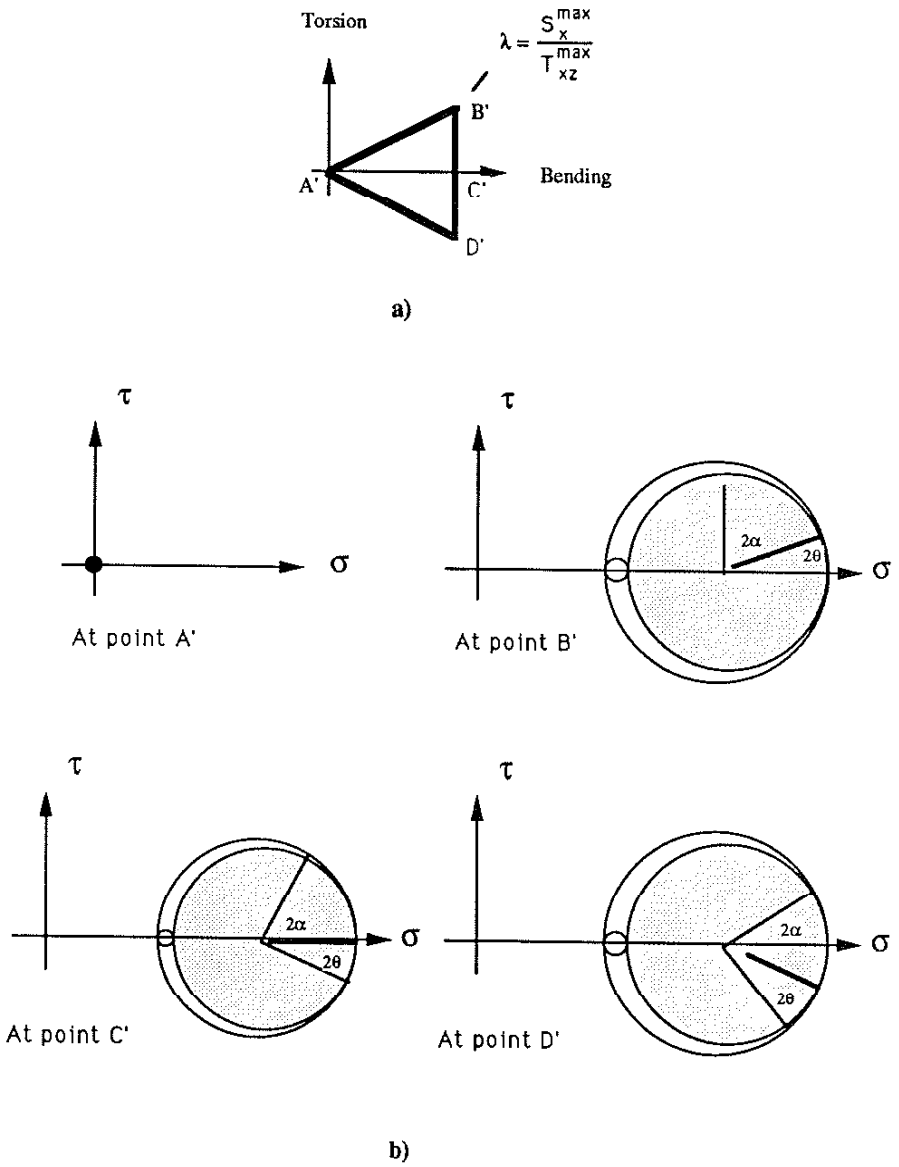

Figure 13 Generalized nominal loading path (a) and local Mohr's stress circles at the critical location below surface for out-of-phase combined bending-torsion (b). Shaded circles represent the surface plane of the notch in three-dimensional stress space.

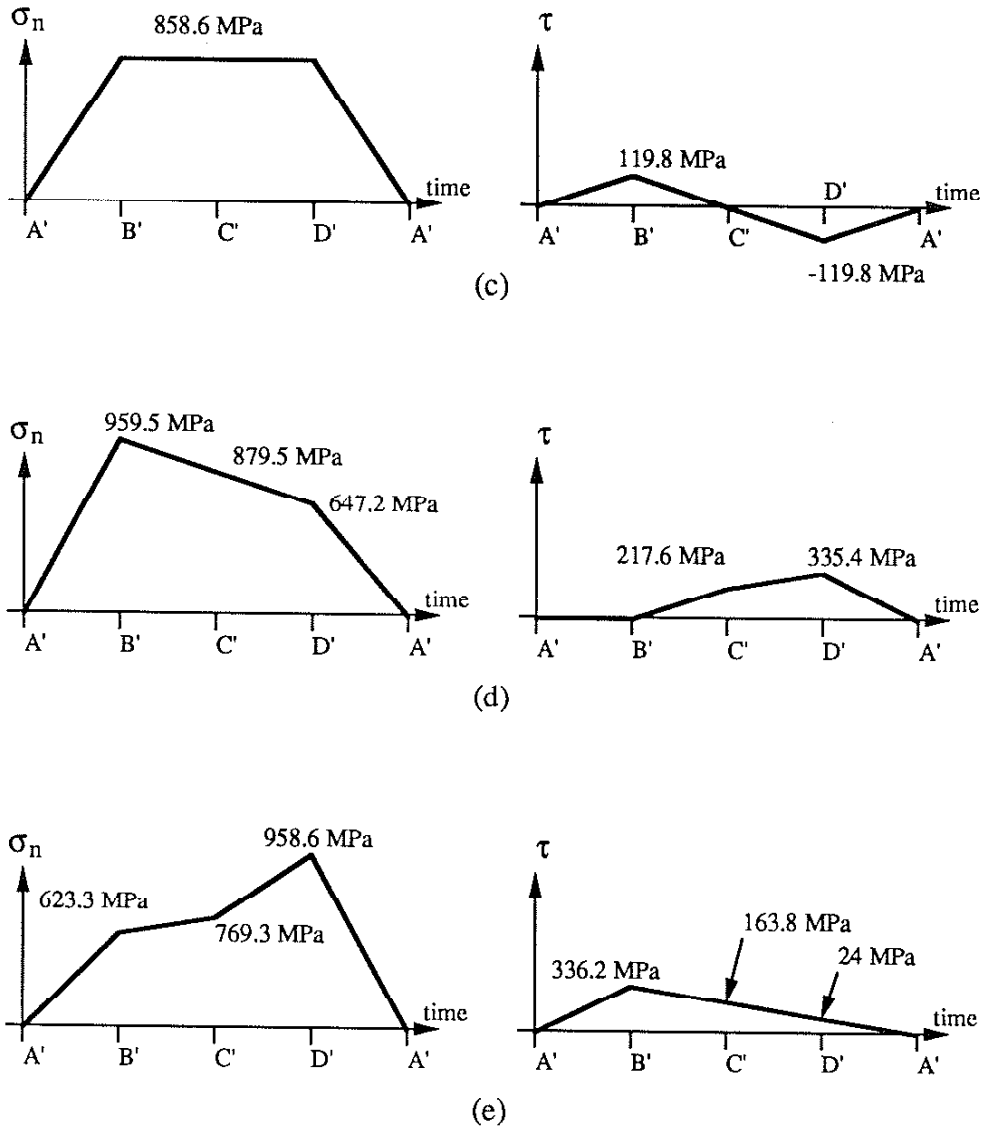

Figure 13 (Continued) Resulting normal and shearing stress-time histories in (c) longitudinal, (d) maximum local principal stress and (e) maximum local shear stress directions corresponding to the out-of-phase bending-torsion loading path shown in Fig. 13a.

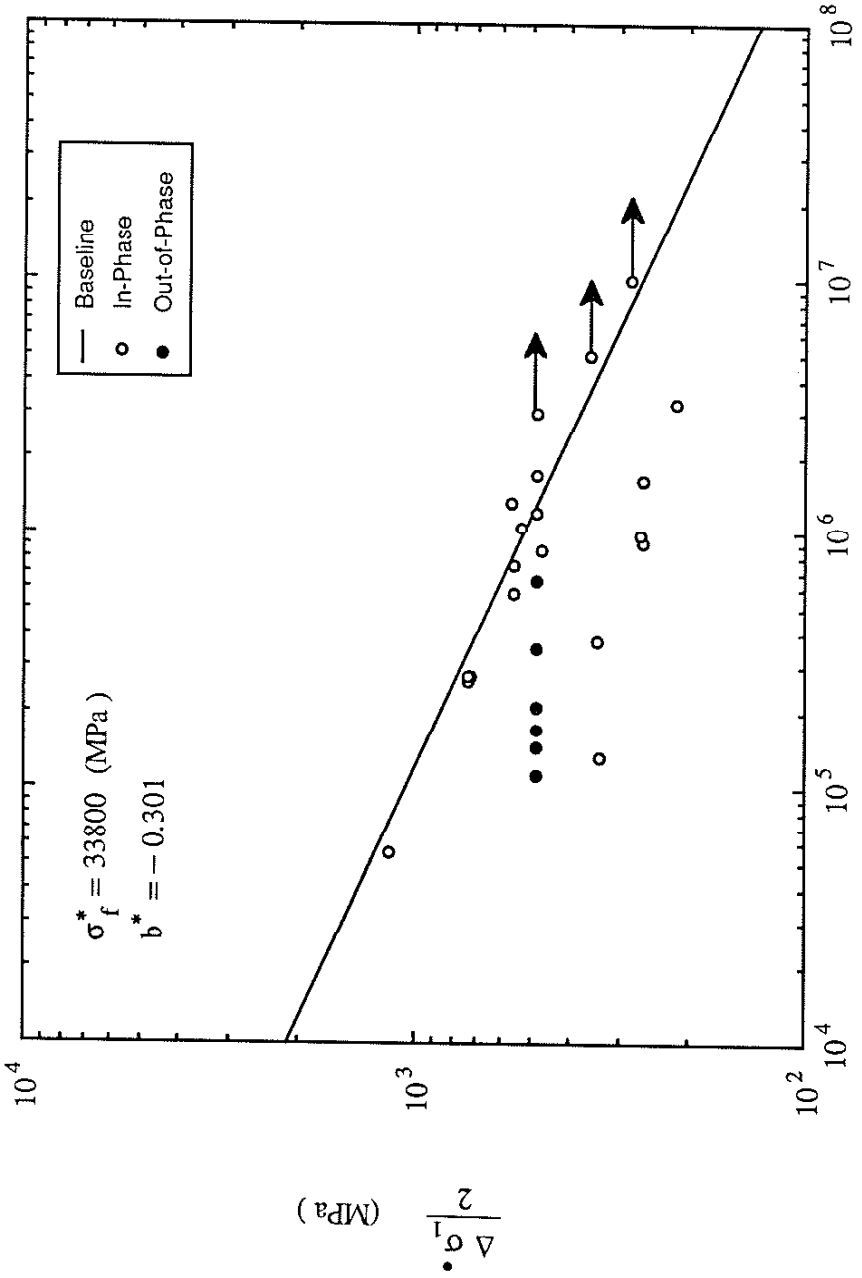

Figure 14 Maximum local principal stress amplitude with Morrow's mean stress correction versus cycles to failure. Mean stresses are assumed to be fully effective throughout the total fatigue life.

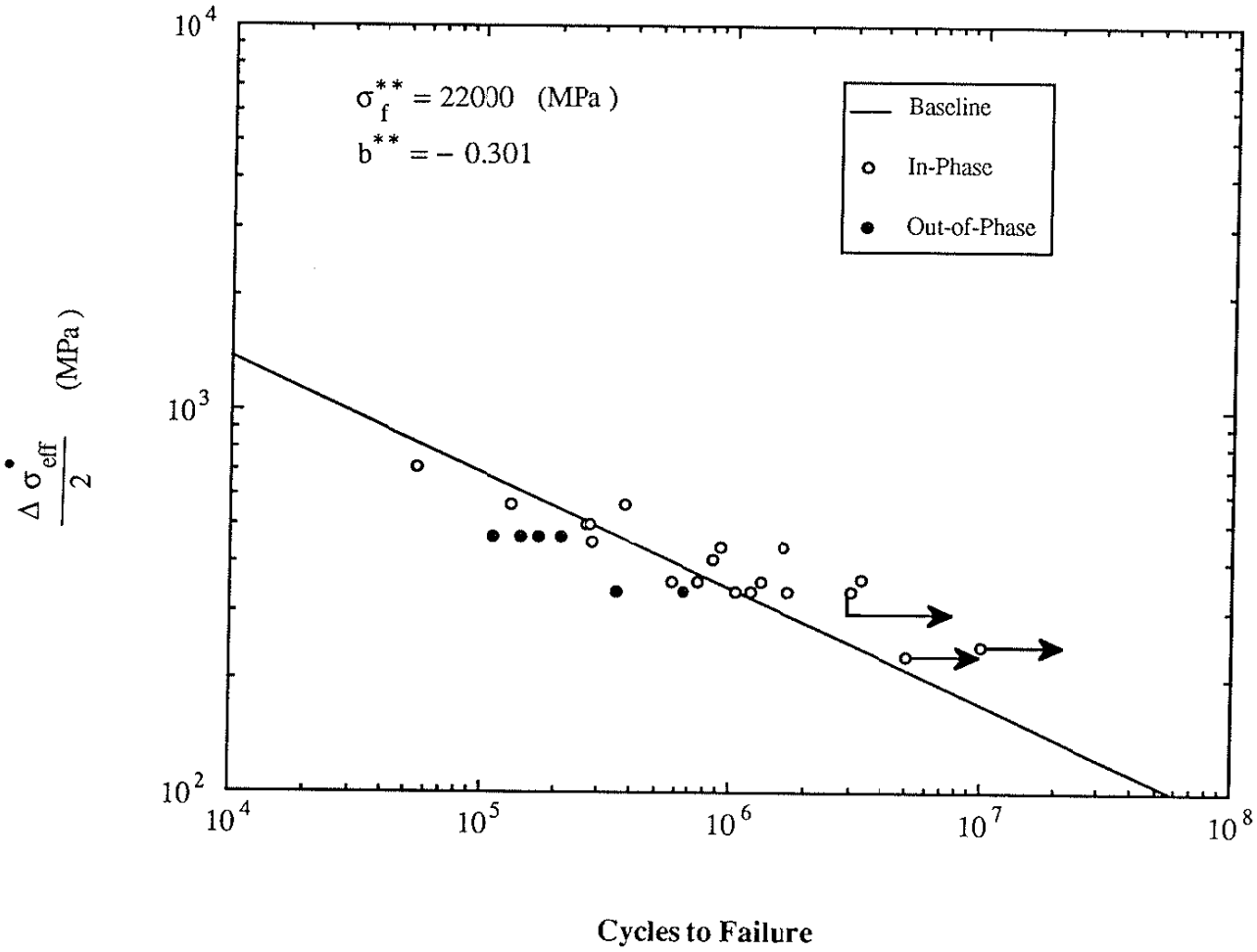

Figure 15 Maximum local von Mises effective stress amplitude with Morrow's mean stress correction versus cycles to failure. Mean stresses are assumed to be fully effective throughout the total fatigue life.

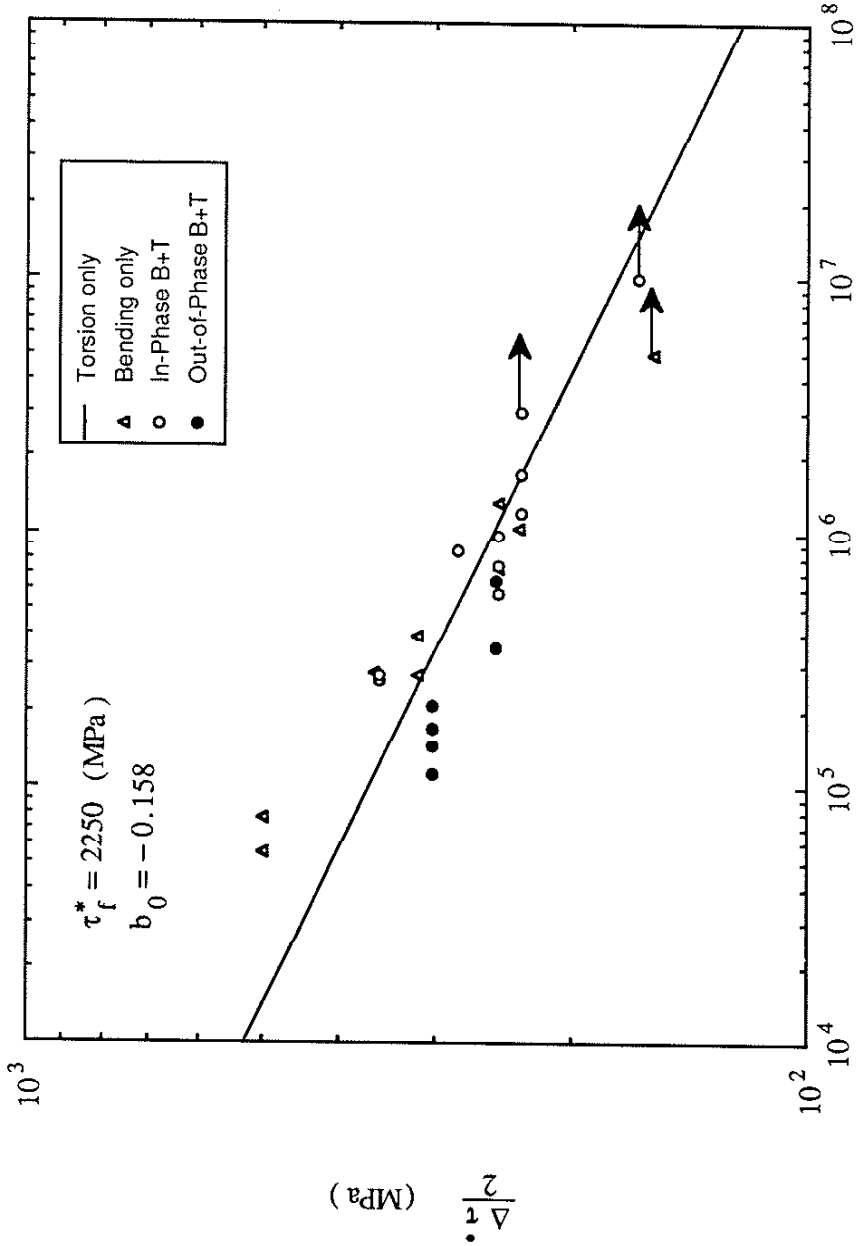

Figure 16 Findley's equivalent local shear stress amplitude versus cycles to failure. Mean normal stresses are assumed to be relaxed early in life (i.e. $\sigma_n^{mean} = 0$).

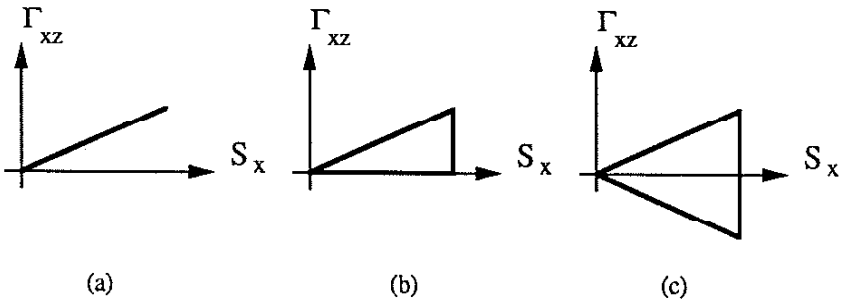

(a) (b) (c)

Experimentally:

$$N_f^a = N_f \qquad N_f^b = \frac{1}{5} N_f \qquad N_f^c = \frac{1}{10} N_f$$

Theoretically:

Local principal stress amplitude with Morrow's mean stress correction:

$$N_f^a = N_f^b = N_f^c$$

Local von Mises effective stress amplitude with Morrow's mean stress correction:

$$N_f^a = N_f^b > N_f^c$$

Local Findley's effective shear stress amplitude ($\sigma_n^{mean} = 0$):

$$N_f^a > N_f^b > N_f^c$$

Figure 17 Overview of the predictive capability of the three fatigue damage parameters investigated in this study.

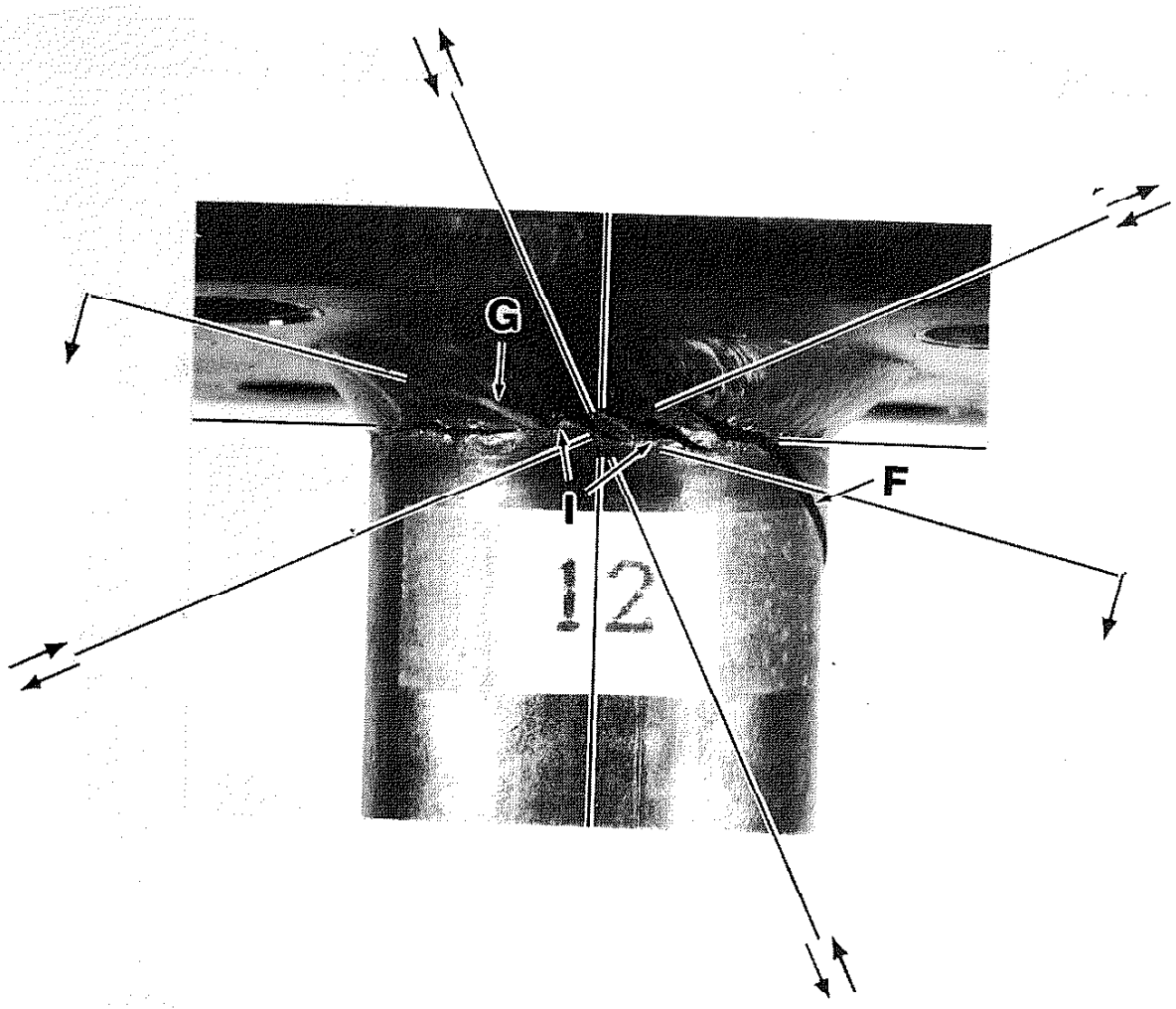

Figure 18 Typical macroscopic cracking behavior for in phase loading, $\lambda = 2.39$ (specimen #12).

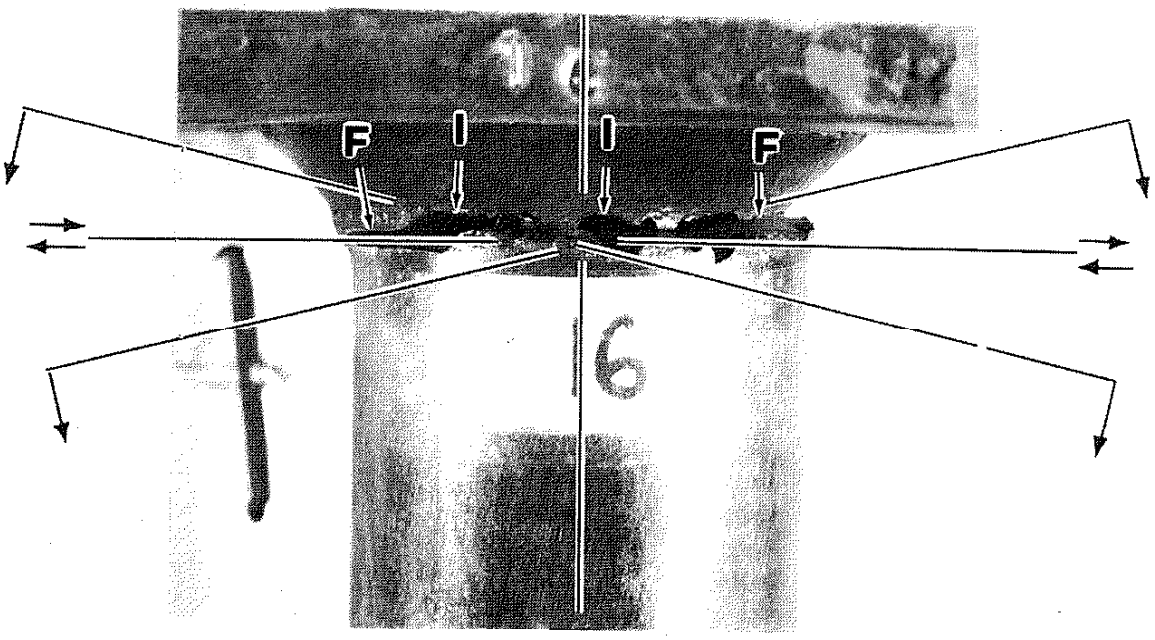

Figure 19 Typical macroscopic cracking behavior for out-of-phase loading, $\lambda = 2.39$ (specimen #16).

APPENDIX A

CALCULATION OF NOMINAL BENDING AND SHEARING STRESS MAGNITUDES IN THE TUBE-TO-PLATE WELDED SPECIMEN

The predetermined nominal bending stress at the weld toe location was calculated as (Fig. A-1):

$$S_x = \frac{\left(F_A^B + F_B^B\right)}{W_x} X_{toe} \tag{A-1}$$

Eq. A-1 was then solved for actuator loads as:

$$\left(F_A^B + F_B^B\right) = \frac{S_x \; W_x}{X_{toe}} \tag{A-2}$$

Hence the load per actuator becomes:

$$\frac{F^B}{\text{actuator}} = \frac{\left(F_A^B + F_B^B\right)}{2} \tag{A-3}$$

Similarly, the predetermined nominal torsional stress was calculated as follows:

$$\Gamma_{xz} = \frac{\left(F_A^T + F_B^T\right)}{W_T} X \tag{A-4}$$

$$\left(F_A^T + F_B^T\right) = \frac{\Gamma_{xz} \; W_T}{X} \tag{A-5}$$

$$\frac{F^T}{\text{actuator}} = \frac{\left(F_A^T + F_B^T\right)}{2} \tag{A-6}$$

Eventually, the total actuator loads were taken as a linear sum of the bending and torsional components of the actuator loads:

$$F_A^{tot} = \frac{F^B}{\text{actuator}} + \frac{F^T}{\text{actuator}} \qquad \text{(actuator A)} \tag{A-7}$$

$$F_B^{tot} = \frac{F^B}{\text{actuator}} - \frac{F^T}{\text{actuator}} \qquad \text{(actuator B)} \tag{A-8}$$

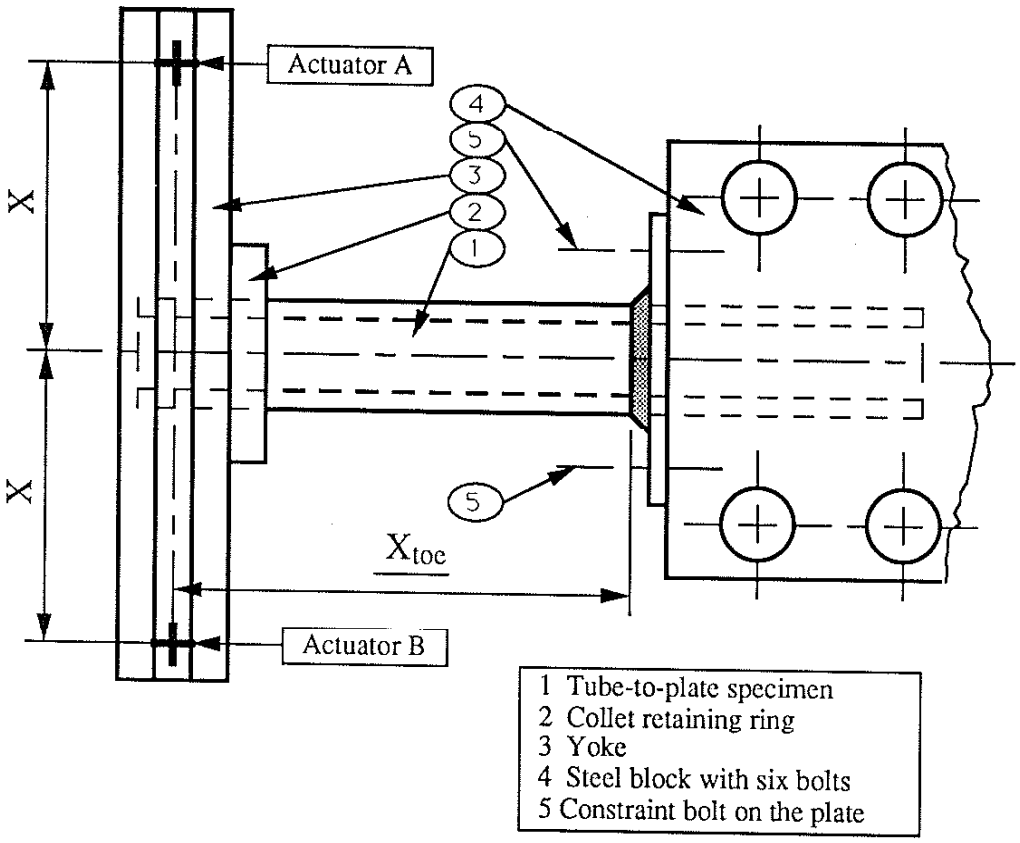

Figure A-1 Schematic representation of the collet-yoke arrangement and the nomenclature employed in Eqns. A-1 through A-5.

APPENDIX B

CALCULATION OF BENDING AND SHEARING STRESS MAGNITUDES IN A SIMPLY SUPPORTED BRIDGE BEAM

In order to calculate the range of bending-shear stress ratios in the 30-WF-124 I-beam, the following assumptions were used. The shear forces V_1 and V_2 can be calculated at any location in a simply supported I-beam as follows (Fig. B-1):

$$V_1 = \frac{P \cdot n}{l} \quad ; x < m \tag{B-1}$$

$$V_2 = \frac{P \cdot m}{l} \quad ; x > m \tag{B-2}$$

$$V_1 + V_2 = P \tag{B-3}$$

Resulting bending moments were calculated as follows:

$$M_x = \frac{P \cdot n \cdot x}{l} \; ; \; x < m \tag{B-4}$$

$$M_{max} = \frac{P \cdot n \cdot m}{l} \; ; \; x = m \tag{B-5}$$

A linear elastic formula was employed to calculate the nominal bending stresses at the web-flange intersection of the I-beam (Fig. B-2):

$$S_x^{max} = \frac{M_{max}}{I} \cdot y \tag{A-6}$$

A nominal shear stress distribution described in Ref. [B1] was assumed for the I-beam cross section. The area of the web rather than the entire area was used. At the web-flange intersection, the following form results:

$$\Gamma_{xz}^{max} = 0.8 \cdot \frac{V_{max}}{A_{web}} \tag{B-7}$$

The values for the bending moment (M) and the two shearing forces (V_1 and V_2) were taken at the center span and 0.1 x span length in the beam to calculate the S_x and Γ_{xz} histories shown in Fig. B-3, as the load (P) crossed the beam.

REFERENCES

B1. Lipson, C., and Juvinall, R. C., Handbook of Stress and Strength, Design and Material Applications, The Macmillan Company, New York, 1963, pp. 15-18.

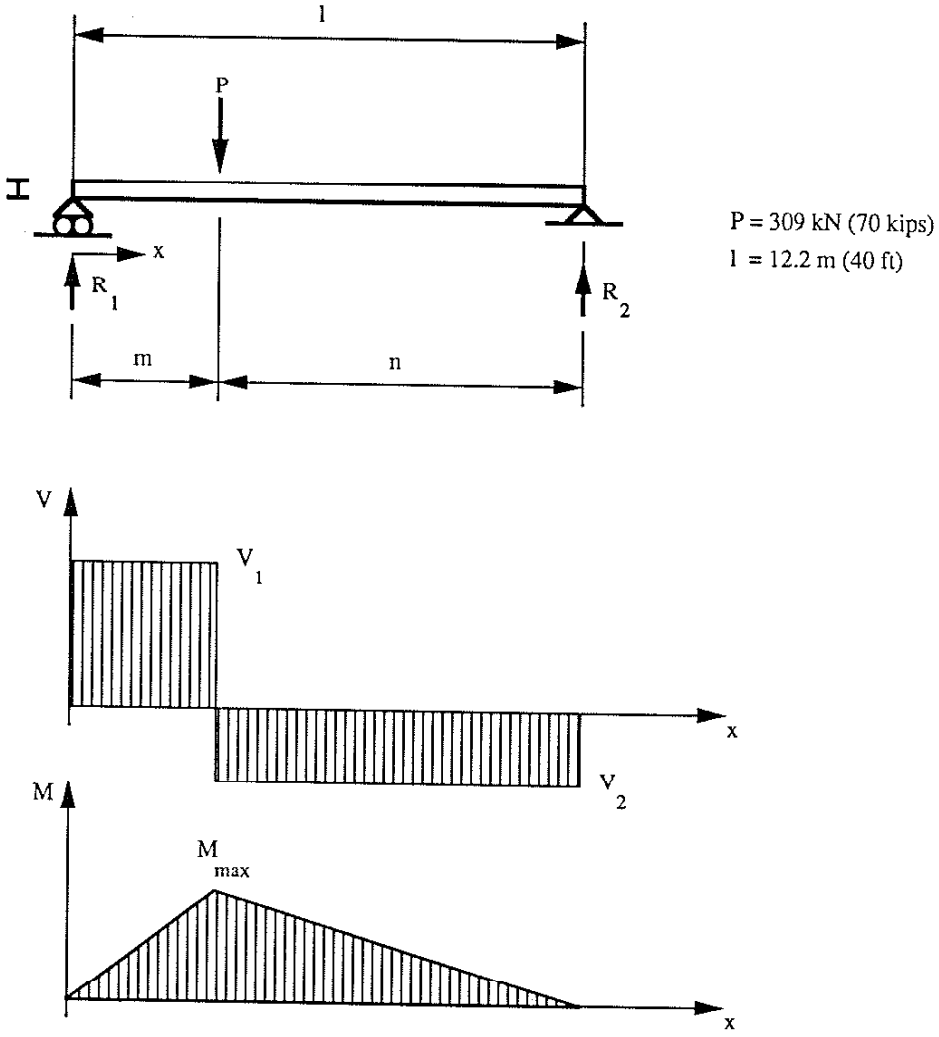

Figure B-1 Generalized shear and moment diagrams for a simply supported bridge beam.

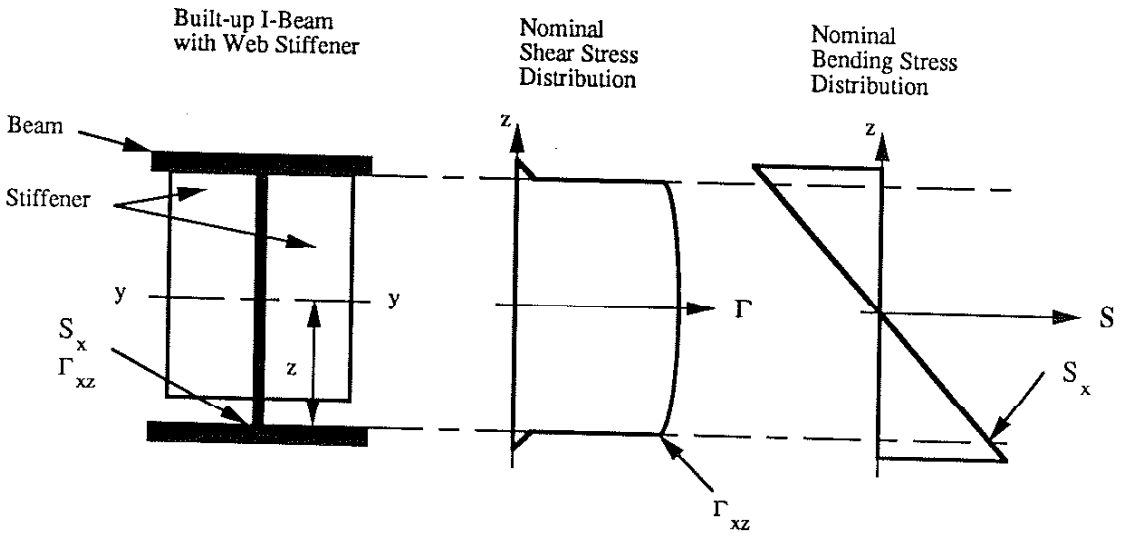

z = 359.41 mm (14.15 in.)

A_{web} = 10680 mm^2 (16.5555 in^2)

Figure B-2 Assumed bending and shear stress distributions and locations used in the calculations.

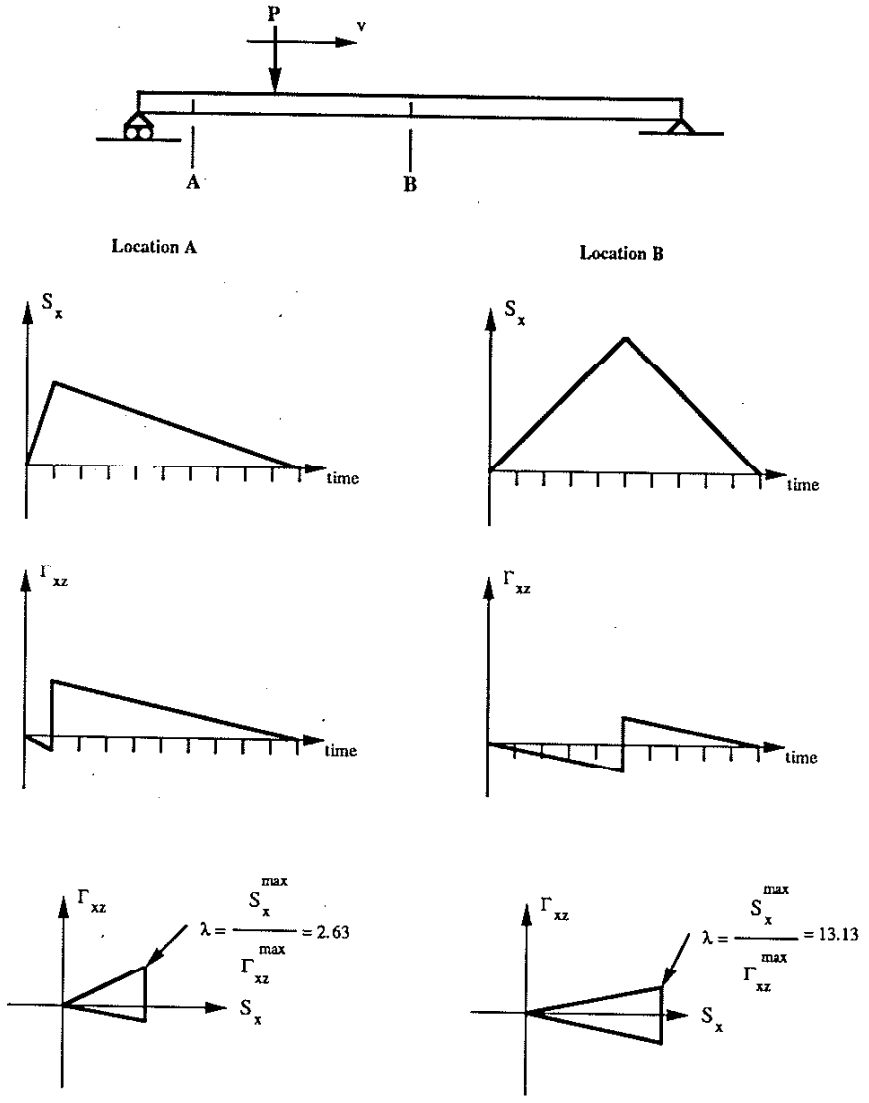

Figure B-3 Typical bending and shearing out-of-phase stress histories for the bridge beam with a moving load.